AD-A225 817

TRIMIX: A VORTICITY-STREAM FUNC-TION APPROACH TO CALCULATING THREE-DIMENSIONAL MIXING FOR VISCOUS, PARABOLIC FLOWS

Peter G. Crowell

R & D Associates
Albuquerque, New Mexico 87119

DTIC FILE COPY

July 1990

Final Report

Approved for public release; unlimited distribution.

DTIC
ELECTE
AUG 24 1990

Weapons Laboratory
Air Force Systems Command
Kirtland Air Force Base, NM 87117-6008

02

This final report was prepared by R & D Associates, Albuquerque, New Mexico, under Contract F29601-87-C-0005, Job Order ILIR8813, with the Weapons Laboratory, Kirtland Air Force Base, New Mexico. Captain Thomas Gregory Gates (ARD) was the Laboratory Project Officer-in-Charge.

When Government drawings, specifications, or other data are used for any purpose other than in connection with a definitely Government-related procurement, the United States Government incurs no responsibility or any obligation whatsoever. The fact that the Government may have formulated or in any way supplied the said drawings, specifications, or other data, is not to be regarded by implication, or otherwise in any manner construed, as licensing the holder or any other person or corporation; or as conveying any rights or permission to manufacture, use, or sell any patented invention that may in any way be related thereto.

This report has been authored by a contractor of the United States Government. Accordingly, the United States Government retains a nonexclusive, royalty-free license to publish or reproduce the material contained herein, or allow others to do so, for the United States Government purposes.

This report has been reviewed by the Public Affairs Office and is releasable to the National Technical Information Service (NTIS). At NTIS, it will be available to the general public, including foreign nationals.

If your address has changed, if you wish to be removed from our mailing list, or if your organization no l··ger employs the addressee, please notify WL/ARD, Kirtland AFB, NM 87117-6008 to help us maintain a current mailing list.

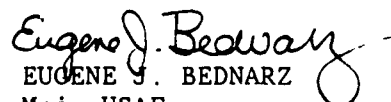This technical report has been reviewed and is approved for publication.

THOMAS GREGORY GATES
Capt, USAF
Project Officer

FOR THE COMMANDER

ROBERT A. HILDRETH
Maj, USAF
Chief, Advanced Concepts Br

EUGENE J. BEDNARZ
Maj, USAF
Acting Chief, Devices Div

1. AGENCY USE ONLY (Leave blank)	2. REPORT DATE July 1990	3. REPORT TYPE AND DATES COVERED Final 01 Mar 88 - 31 Dec 89

4. TITLE AND SUBTITLE
TRIMIX: A VORTICITY-STREAM FUNCTION APPROACH TO CALCULATING THREE-DIMENSIONAL MIXING FOR VISCOUS, PARABOLIC FLOWS

6. AUTHOR(S)
Crowell, Peter G.

5. FUNDING NUMBERS
C: F29601-87-C-0005
PE: 61101F
PR: ILIR
TA: 88
WU: 13

7. PERFORMING ORGANIZATION NAME(S) AND ADDRESS(ES)
R & D Associates
Albuquerque, NM 87119

8. PERFORMING ORGANIZATION REPORT NUMBER

9. SPONSORING/MONITORING AGENCY NAME(S) AND ADDRESS(ES)
Weapons Laboratory
Kirtland AFB, NM 87117-6008

10. SPONSORING/MONITORING AGENCY REPORT NUMBER
WL-TR-90-19

11. SUPPLEMENTARY NOTES

12a. DISTRIBUTION/AVAILABILITY STATEMENT
Approved for public release; distribution unlimited.

12b. DISTRIBUTION CODE

13. ABSTRACT (Maximum 200 words)

A 3D computer code (TRIMIX) has been developed to predict the influence of axial vorticity and diffusional velocity model on the rate of mixing between a primary flow and an injected secondary flow. Computational results are presented for the gain and iodine dissociation in an oxygen/iodine laser and compared with results obtained using the 1D premixed approximation. The premixed model significantly underpredicts laser performance; and the binary diffusion model and the zero vorticity approximation both lead to large error in the predicted gain.

14. SUBJECT TERMS
Computation Fluid Dynamics   Jets
Mixing   Vorticity

15. NUMBER OF PAGES
66

16. PRICE CODE

17. SECURITY CLASSIFICATION OF REPORT	18. SECURITY CLASSIFICATION OF THIS PAGE	19. SECURITY CLASSIFICATION OF ABSTRACT	20. LIMITATION OF ABSTRACT
Unclassified	Unclassified	Unclassified	

TABLE OF CONTENTS

LIST OF ILLUSTRATIONS

SECTION 1

INTRODUCTION

One of the most difficult fluid dynamic analysis problems, in the design of chemical lasers, is the computation of the mixing between the primary flow and various injected secondary flows. The exact calculation of the mixing process requires the solution of the three-dimensional (3-D) Navier-Stokes equations for a chemically reacting, viscous, compressible flow over a very fine mesh. Due to the tight mesh requirements and the need to solve large numbers of species equations, exact solutions require hundreds of hours of computer time per case, even on CRAY class machines. As a consequence, chemical laser mixing analyses have been done almost exclusively using the two-dimensional (either axisymmetric or planar 2-D) parabolic, thin shear layer approximation (Ref. 1). When the secondary flow is injected parallel to the primary flow, the 2-D approach is valid. However, in most instances, the sidewall injection concept is used wherein the secondary flow is injected into the primary at some large angle. In this instance, the bending of the injected jet in the direction of the primary flow induces a large axial vorticity (i.e., flow swirl) component into the jet. Since the 2-D equations have zero axial vorticity by definition, there is every reason to believe that the 2-D approach will underpredict the rate at which the two flows will mix.

The rate at which mixing takes place is dependent upon the magnitude of the convective velocities transverse to the flow direction and the magnitude of the diffusional velocities. With the 2-D shear layer equations, the transverse convective velocity is small and the choice of a model for the diffusional velocities (i.e., binary diffusion versus multicomponent diffusion) has a significant influence on the computed results (Ref. 1). However, for the 3-D equations with large axial vorticity, the magnitude of the transverse convective velocities can be of the same order as the velocity in the flow direction. In this situation, the influence of the model for the diffusional velocities may be much

1

less dominant than for the 2-D case. Since the choice of model for the diffusional velocities has a first-order impact on the computational expense, some assessment of its impact on the rate of mixing in flows with large axial vorticity is required.

This report discusses the development of a 3-D mixing code (TRIMIX) to predict the influence of axial vorticity and diffusional velocity model on the rate of mixing between the primary flow and an injected secondary flow. The parabolic flow approximation will be used to minimize computation time and the initial distribution of axial vorticity will be specified. Therefore, the calculation will not be exact since the initial vorticity distribution will not be known exactly. However, the experimental data base on sidewall injection is sufficient to make a reasonable estimate of the initial vorticity. The resulting code is expected to run between one and two orders of magnitude faster than a Navier-Stokes calculation (3 to 5 h of CRAY time for a chemically reacting flow).

SECTION 2
ANALYSIS

A typical chemical laser nozzle is shown in Figure 2.1 with sidewall injection from both walls in the subsonic flow region. Also shown is a commonly used injection pattern with two rows of staggered holes. The number of rows, hole sizes and spacing are chosen to provide a uniform distribution of the secondary flow throughout the primary flow. A rectangular coordinate system will be used with x in the primary flow direction, y perpendicular to the nozzle axis and z in the direction along which the injection holes are spaced. The corresponding velocity components are u in the x direction, v in the y direction and w in the z direction. The number of holes in the z direction generally ranges from 20 to 50. Since it takes at least 20 mesh points in the z direction to resolve the flow field from one hole to the next, and about 40 in the y direction from y = o to y = H, it is obvious that carrying out the computation over the entire array of holes would be prohibitively expensive. Fortunately, in most instances the hole pattern in the z direction is symmetric such that the computations can be carried out for a unit cell of width Δ (see Fig. 2.1). Therefore, the computational domain in the z direction is from z = o to z = $\Delta(x)$. Since the walls which bound the flow in the z direction are generally not parallel to one another, Δ must vary in the x direction to conserve the cross-sectional flow area. The injection pattern from the top wall (y = H) is usually staggered from the hole pattern at y = -H such that the flow is not symmetric about y = o. However, to conserve computation time, in this report y = o will be assumed to be a symmetry plane and the computational domain in the y direction is from y = o to y = H(x).

2.1 EQUATIONS.

To satisfy the continuity equation, two stream functions are defined as follows:
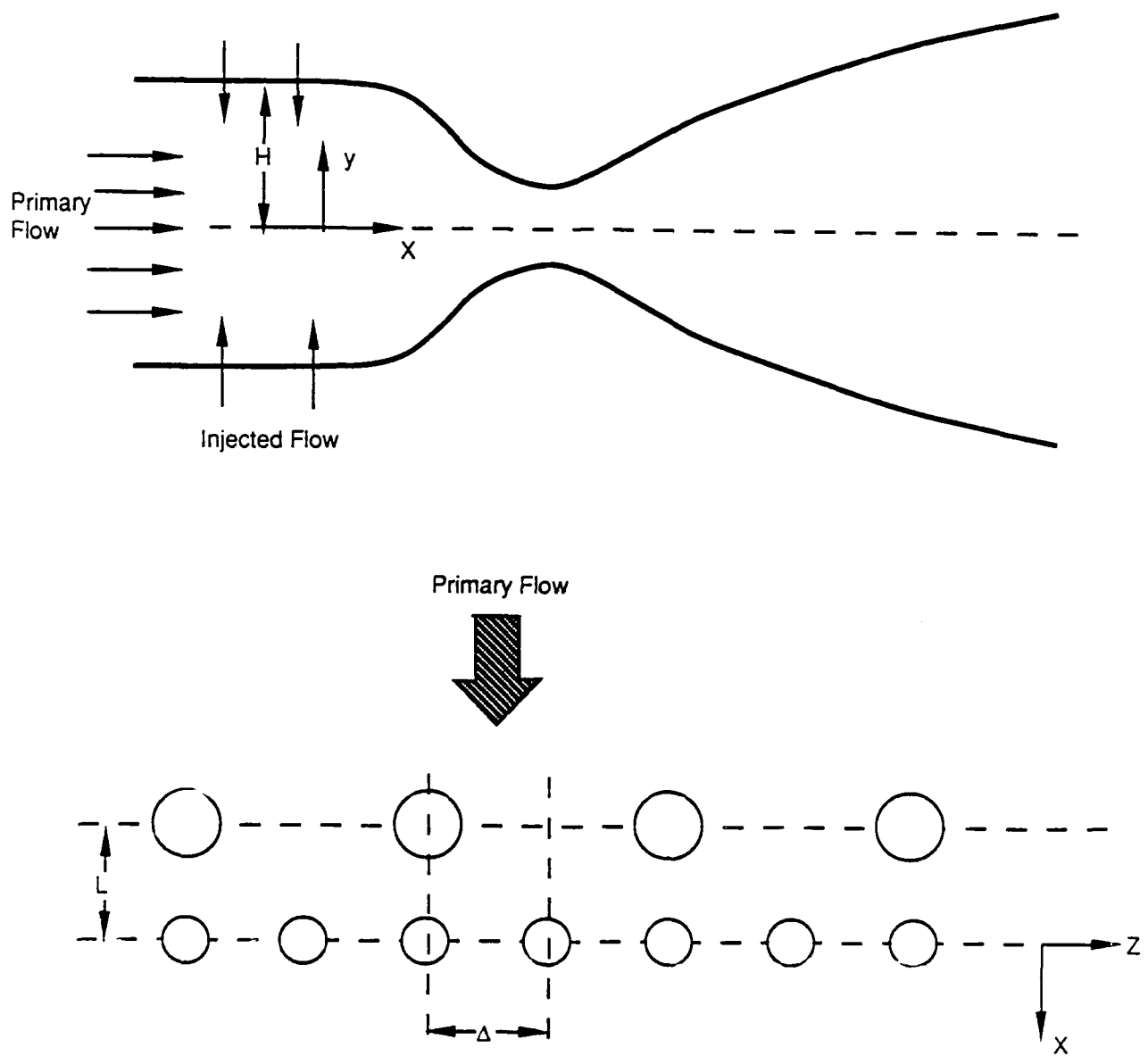
Figure 2.1.   Nozzle geometry and injection hole pattern.

$$\frac{\partial \Psi}{\partial y} \equiv - \rho w \qquad \frac{\partial \psi}{\partial y} \equiv - \frac{\partial}{\partial x}(\rho u) \qquad (2.1)$$

The remaining velocity component v is defined by:

$$\rho v = \frac{\partial \Psi}{\partial z} + \psi \qquad (2.2)$$

The axial vorticity (i.e., the x vorticity component) is defined by:

$$\omega \equiv \frac{\partial w}{\partial y} - \frac{\partial v}{\partial z} \qquad (2.3)$$

where the vorticity is defined to be positive for clockwise rotation.

Substitution of the v and w expressions of Equations 2.1 and 2.2 into Equation 2.3 provides the equation for the stream function Ψ.

$$\frac{\partial^2 \Psi}{\partial y^2} + \frac{\partial^2 \Psi}{\partial z^2} - \left(\frac{1}{\rho} \frac{\partial \rho}{\partial y}\right) \frac{\partial \Psi}{\partial y} - \left(\frac{1}{\rho} \frac{\partial \rho}{\partial z}\right) \frac{\partial \Psi}{\partial z}$$

$$= - \rho \omega + \left(\frac{1}{\rho} \frac{\partial \rho}{\partial z}\right) \psi - \frac{\partial \psi}{\partial z} \qquad (2.4)$$

The momentum equation in the x direction is used to solve for the u velocity component and is given by:

$$\rho \mathbf{V} \cdot \nabla u = \nabla \cdot (\mu \nabla u) - \mathcal{P} \qquad (2.5)$$

$$\mathcal{P} \equiv \frac{dp}{dx}$$

This equation is parabolized by dropping the x derivative in the divergence of $\mu \nabla u$ and by replacing the pressure gradient term by the derivative of the mean pressure. That is, the pressure gradient ($\mathcal{P}$) is some average value over the flow cross section and is chosen to satisfy global continuity in the form of Equation 2.6.

5

$$\dot{r} = \int_0^H \int_0^\Delta \rho u \, dz \, dy = \text{constant} \tag{2.6}$$

Equations 2.5 and 2.6 are two coupled equations which are solved for u and $\wp$. After solving for u, the stream function ψ of Equation 2.1 is evaluated by integration:

$$\psi = - \int_0^Y \frac{\partial}{\partial x}(\rho u) \, dy \tag{2.7}$$

The transport equation for axial vorticity for a compressible, variable viscosity fluid is derived in Appendix A and is given as (Equation A.6):

$$\rho \mathbf{V} \cdot \nabla \omega = \nabla \cdot (\mu \nabla \omega) - \omega \frac{\partial \psi}{\partial y} + \Omega \tag{2.8}$$

where the subscript x has been dropped from ω_x and Equation 2.1 has been used to introduce the stream function ψ. The quantity Ω is defined in Equation A.6 of Appendix A and contains the terms involving the gradients in density and viscosity.

The species equations are given by:

$$\rho \mathbf{V} \cdot \nabla K_i = - \nabla \cdot (\rho K_i \mathbf{V}_i) + w_i \tag{2.9}$$

where K_i is the species mass fraction, $\dot{w}_i$ is the net rate of production of species i due to chemical reactions and $\mathbf{V}_i$ is the species diffusional velocity vector and is defined by:

$$\mathbf{V}_i = \hat{v}_i \, \mathbf{e}_y + \hat{w}_i \, \mathbf{e}_z \tag{2.10}$$

where axial diffusion is ignored due to the parabolic flow approximation.

6

As indicated earlier, one of the objectives of this effort is to assess the influence of the diffusional velocity model on the computed results. In Reference 2, it was demonstrated that the "effective" binary diffusion model gave results which were in excellent agreement with the exact multicomponent diffusion model. Since the "effective" binary diffusion model requires much less computational effort than solving the Stefan-Maxwell equations for the multicomponent model, the effective binary diffusion model is used to define the diffusional velocities. The diffusional velocities are given as:

$$K_i M \hat{v}_i = - D_i \nabla_y (K_i M) + K_i \sum_{J=1}^{N} D_j \nabla_y (K_j M) + S_i \nabla_y P/P$$

$$K_i M \hat{w}_i = - D_i \nabla_z (K_i M) + K_i \sum_{J=1}^{N} D_j \nabla_z (K_j M) + S_i \nabla_z P/P$$

$$S_i \equiv - D_i K_i (1 - M_i/M) + K_i \sum_{J=1}^{N} D_j K_j (1 - M_j/M) \qquad (2.11)$$

where ∇_y denotes the gradient operator in the y direction and ∇_z in the z direction. M is the mixture molecular weight. Reference 3 may be consulted for the derivation of Equation 2.11. The diffusion coefficient is given by:

$$D_i = (1 - x_i)/\left[p \sum (x_j/pD_{ji}) \right] \qquad (2.12)$$

where x_i is the mole fraction of species i and the D_{ji} are the binary diffusion coefficients. Note that the summation of Equation 2.12 excludes j = i.

For comparative purposes, the code also contains the binary diffusion model with the diffusional velocities given by:

7

$$K_i \hat{v}_i = - D\nabla_y(K_i) \qquad\qquad K_i \hat{w}_i = - D\nabla_z(K_i)$$

$$D \equiv \mu/\rho Sc \qquad\qquad\qquad\qquad (2.13)$$

where Sc is the Schmidt number.

The energy equation is solved for temperature and is given by:

$$\rho C_p \mathbf{v}\cdot\nabla T = \nabla\cdot(K\nabla T) + \mathbf{v}\cdot\nabla p + \mu\nabla u\cdot\nabla u +$$

$$- \rho \sum_{i=1}^{N} K_i C_{p_i} (\mathbf{v}_i \cdot \nabla T) - \sum_{i=1}^{N} h_i \dot{w}_i \qquad (2.14)$$

Again, this expression is parabolized by ignoring axial heat conduction and by ignoring the x derivative in the viscous dissipation term.

The pressure gradients required to calculate the pressure diffusion of Equation 2.11 and the flow work of Equation 2.14 are obtained from the primitive variable form of the y and z momentum equation and are given by:

$$\frac{\partial P}{\partial y} = \nabla\cdot(\mu\nabla v) - \rho(\mathbf{v}\cdot\nabla)v$$

$$\frac{\partial P}{\partial z} = \nabla\cdot(\mu\nabla w) - \rho(\mathbf{v}\cdot\nabla)w \qquad (2.15)$$

2.2 BOUNDARY CONDITIONS.

As indicated in Section 2, the planes y = o, z = o and z = Δ are symmetry planes. Therefore, at y = o, the y gradients in axial velocity, temperature and species vanish. At z = o and z = Δ, the z gradients in axial velocity, temperature and species vanish. At y = H, there may be either a wall or a plane of symmetry. If a symmetry plane is present at y = H, then the y gradients in velocity, temperature and species are zero. For a wall at y = H,

8

the no-slip condition (u = o) is used for velocity and the wall temperature is specified.

Heterogeneous wall reactions are accounted for in the species boundary conditions at y = H when a wall is present. The boundary condition is:
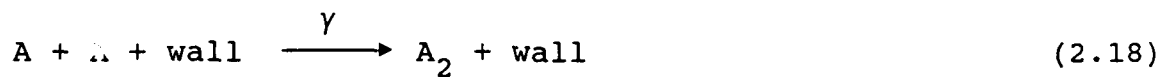
y = H: (for wall)

$$- \rho_w \cos\theta \ K_i \hat{v}_i = \dot{J}_i$$

$$\text{Tan}\theta = \frac{dH}{dx} \ . \tag{2.16}$$

The net rate of species production per unit time and surface area is denoted by $\dot{J}_i$ and is given as:

$$\dot{J}_i = \rho_w \left(RT/2\pi M_i \right)^{1/2} \left[\phi_1 K_i + \phi_2 \right] \tag{2.17}$$

where the specific expressions for ϕ_1 and ϕ_2 depend on the particular wall reactions involving the ith species. For atom wall recombination reactions, the surface reaction is:

$$A + A + \text{wall} \ \xrightarrow{\gamma} \ A_2 + \text{wall} \tag{2.18}$$

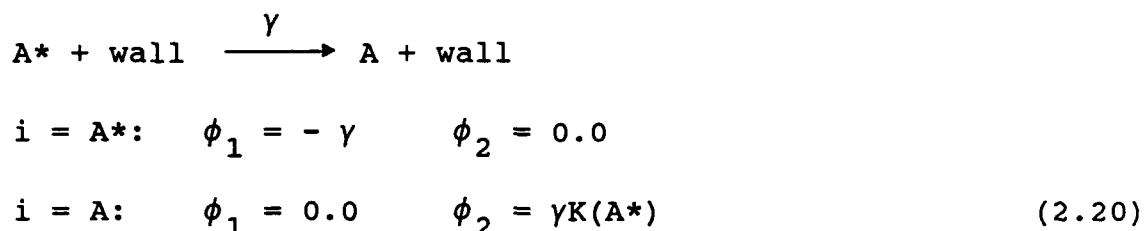For reaction Equation 2.18, the coefficients are:

$$i = A: \ \phi_1 = -\gamma \qquad \phi_2 = \gamma K_{A_2} \left(K_A / K_{A_2} \right)_{eq}$$

$$i = A_2: \ \phi_1 = -\gamma \sqrt{2} \left(K_A / K_{A_2} \right)_{eq} \qquad \phi_2 = \gamma \sqrt{2} \ K_A \tag{2.19}$$

where γ is the recombination coefficient. Note that usually the wall temperature is low enough such that the equilibrium ratio is

vanishing small, in which case $\phi_2(i = A)$ and $\phi_1(i = A_2)$ may be zeroed with negligible error.

For surface deactivation of an excited species A*, the reaction is represented by:

$$A* + wall \xrightarrow{\quad\gamma\quad} A + wall$$

$$i = A*: \quad \phi_1 = -\gamma \qquad \phi_2 = 0.0$$

$$i = A: \quad \phi_1 = 0.0 \qquad \phi_2 = \gamma K(A*) \tag{2.20}$$

The boundary conditions for the axial vorticity and stream functions are obtained from their definitions and a knowledge of the behavior of the v and w velocity components on the boundaries. The v and w velocity components on the boundaries are given by:

$$y = o: \quad v = o \qquad \frac{\partial w}{\partial y} = o$$

$$y = H: \quad v = u\frac{dH}{dx} \qquad w = o \text{ (wall)} \quad \frac{\partial w}{\partial y} = o \text{ (symmetry plane)}$$

$$z = o: \frac{\partial v}{\partial z} = o \qquad w = o$$

$$z = \Delta: \quad \frac{\partial v}{\partial z} = o \qquad w = u\frac{d\Delta}{dx} \tag{2.21}$$

At the symmetry planes $y = o$ and $z = o$, the axial vorticity is zero. At $z = \Delta$, differentiating the boundary condition on w with respect to y gives:

$$z = \Delta: \qquad \omega = \frac{d\Delta}{dx}\frac{\partial u}{\partial y} \tag{2.22}$$

At $y = H$, the axial vorticity is zero if a symmetry plane is present. If a wall is present at $y = H$, then $v = w = o$ and the vorticity is:

$$y = H: \qquad \omega = \frac{-1}{\rho} \frac{\partial^2 \psi}{\partial y^2} \qquad\qquad (2.23)$$

The boundary condition on ψ at $y = 0$ must be consistent with the requirement that $v = 0$ at the symmetry plane. Therefore, $\psi = 0$ at $y = 0$. This condition is incorporated into the expression of Equation 2.7. The derivatives of Ψ with respect to y and z are evaluated on the boundaries using Equations 2.1, 2.2 and 2.21. By integrating these derivatives, the Ψ values on the boundaries can be determined to within an arbitrary constant. Since only the derivatives of Ψ are required to define v and w, the value assigned to the constant is irrelevant. Therefore, we set $\Psi = 0$ at $y = 0$, $z = 0$ to obtain the following:

$$y = 0: \qquad \Psi = 0$$

$$y = H: \qquad \Psi = \frac{dH}{dx} \int_0^z \rho u \, dz - \int_0^z \psi \, dz$$

$$z = 0: \qquad \Psi = 0$$

$$z = \Delta: \qquad \Psi = -\frac{d\Delta}{dx} \int_0^Y \rho u \, dy \qquad\qquad (2.24)$$

2.3 INITIAL CONDITIONS.

Figure 2.2 shows the injected jets corresponding to the hole injection patterns of Figure 2.1. In the immediate region of the injection process (between stations O and D) the problem is elliptic and requires a Navier-Stokes solution to define the flow field. The approach in the TRIMIX code is to start the calculation at some small distance downstream (station D) of the jet injection location where the primary flow has bent the jets approximately parallel to the flow. Since the jets are still essentially unmixed at station D, this seems to be a reasonable way to carry out the 3-D mixing calculation while avoiding the complexity of the exact
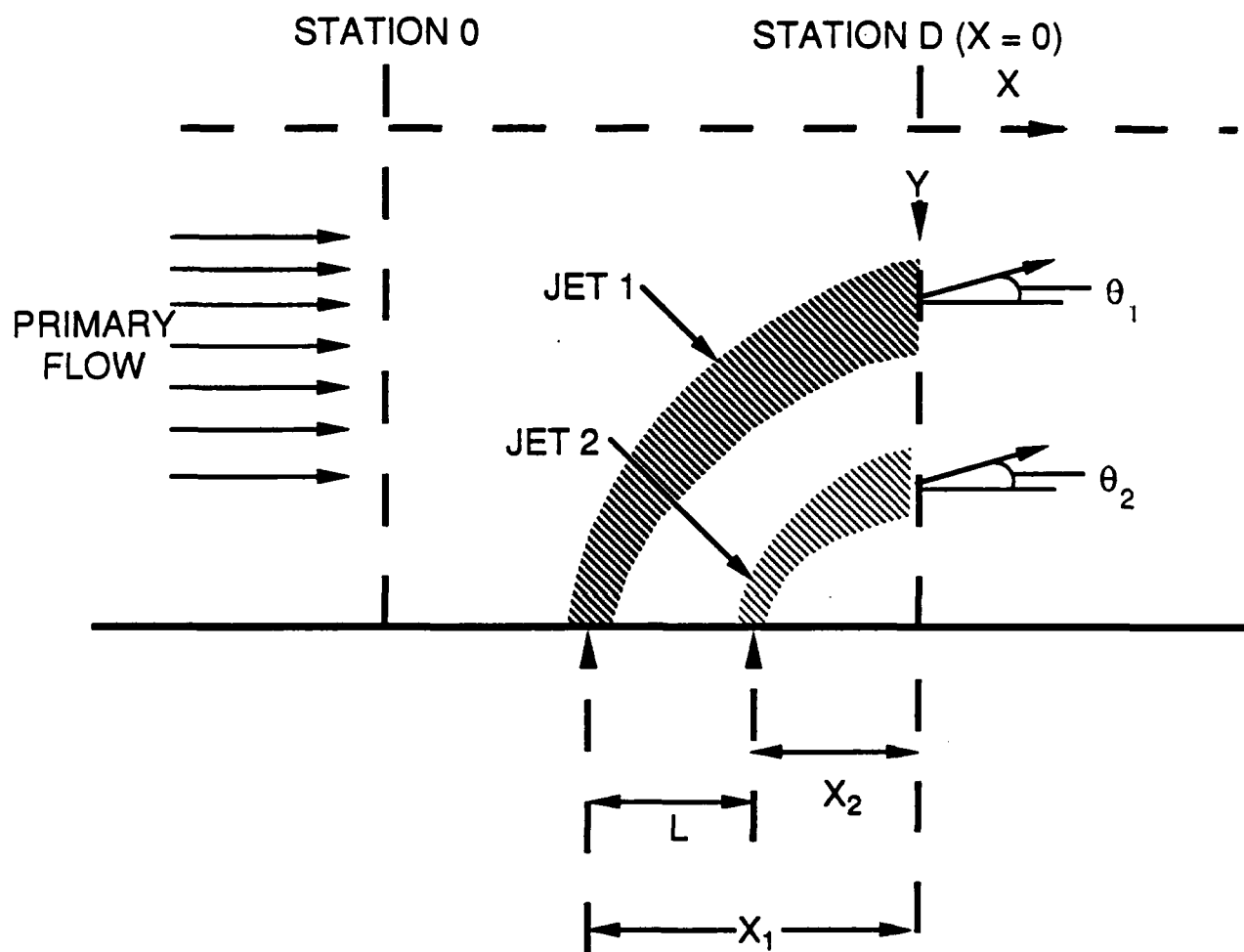
11

Figure 2.2. Schematic of injection geometry.

12

Navier-Stokes calculation. The difficulty with this approach is that it requires the specification of the initial conditions at station D. In Appendix B, the initial conditions for the thermodynamic state variables, the axial velocity (u) and the area occupied by each jet are obtained by satisfying the global conservation equations with some closure assumptions. To obtain the initial axial vorticity and transverse velocity components (v and w), proceed as follows.

Following Fearn and Weston (Ref. 4), we adopt the diffuse vortex model where the distribution of vorticity is assumed to be Gaussian within each vortex. It is also assumed that the jets are spaced far enough apart such that the vorticity field of each jet is independent from that of its neighbors. Thus, the vorticity distribution is taken to be a linear combination of the vorticity field of each jet. This gives:

$$\omega = \sum_{i=1}^{n} \omega_i e^{-\beta_i r^2}$$

$$r^2 = \left(y - y_i\right)^2 + \left(z - z_i\right)^2 \tag{2.25}$$

where r is the radial distance from the center of each vortex with coordinates y_i and z_i. For the injection pattern shown in Figure 2.1, there are three vortices located in the unit computational cell. The vortex locations are shown in Figure 2.3.

The strength of each vortex (Γ) is defined by:

$$\Gamma_i = 2\pi \int_0^\infty \omega_i e^{-\beta_i r^2} \, r \, dr = \pi \omega_i / \beta_i \tag{2.26}$$

The diffusion constant β is defined in terms of the vortex core size by Equation 2.6 of Reference 4 and is reproduced here as:

13
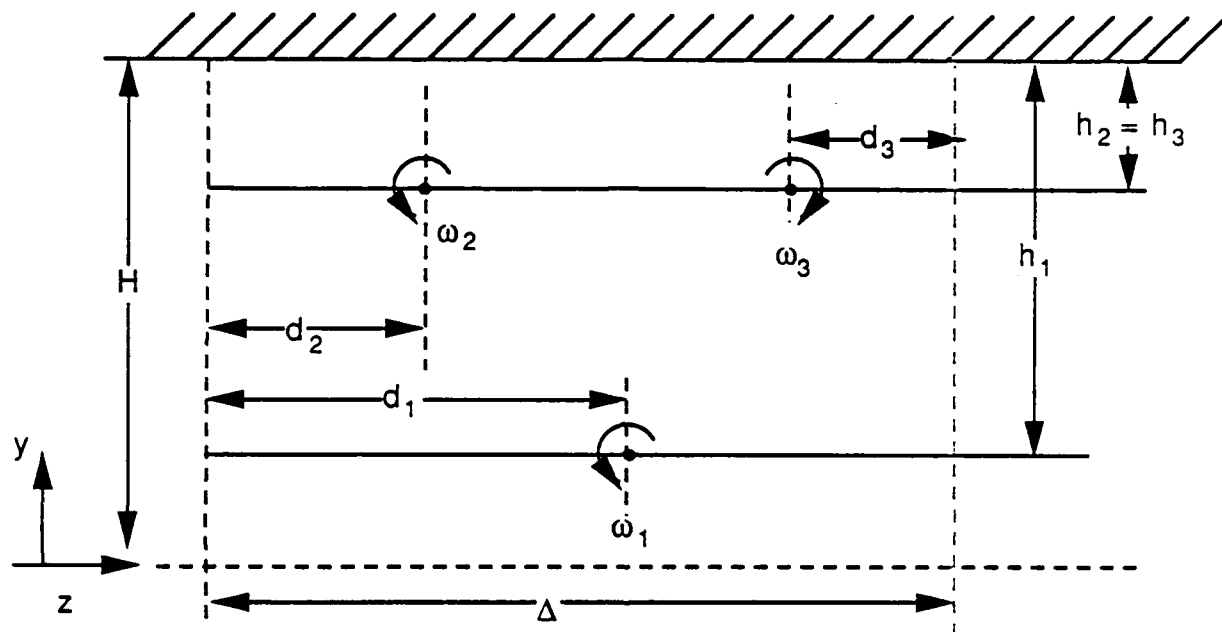
$$\omega_1 < 0 \qquad \omega_2 < 0 \qquad \omega_3 = -\omega_2$$

$$d_2 = d_3$$

Figure 2.3. Initial vortex geometry.

$$\beta = \left(\frac{1.121}{r_c}\right)^2 \tag{2.27}$$

where the β of this report is β^2 of Fearn and Weston.

The vortex core size is obtained from Figure 9 of Reference 4 and is curve fit as:

$$\frac{r_c}{D} = 0.11 \frac{S}{D} + 0.60 \tag{2.28}$$

where S is distance measured along the vortex curve from the injection location to x = o. The distance S is defined in Equation 2.33.

The vorticity at the center, ω_i, is obtained from Equation 2.26 for a given value of the vortex strength Γ_i. The data of Fearn and Weston (Table 2 of Ref. 4) for the initial vortex strength near the jet orifice is plotted in Figure 2.4 for normal injection into a subsonic flow. Also shown is the maximum computed vorticity from the analytical model of Karagozian (Ref. 5). The data are represented by:

$$\Gamma = 1.4 \ DV_\infty R$$

$$R \equiv \left(\rho_J V_J^2 / \rho_\infty V_\infty^2\right)^{1/2} \tag{2.29}$$

where D is the jet orifice diameter, subscript J denotes jet orifice values and subscript ∞ denotes free stream values (i.e., station O in Fig. 2.2). Note that ω_i and Γ_i are defined to be positive for clockwise rotation and negative for counterclockwise rotation.
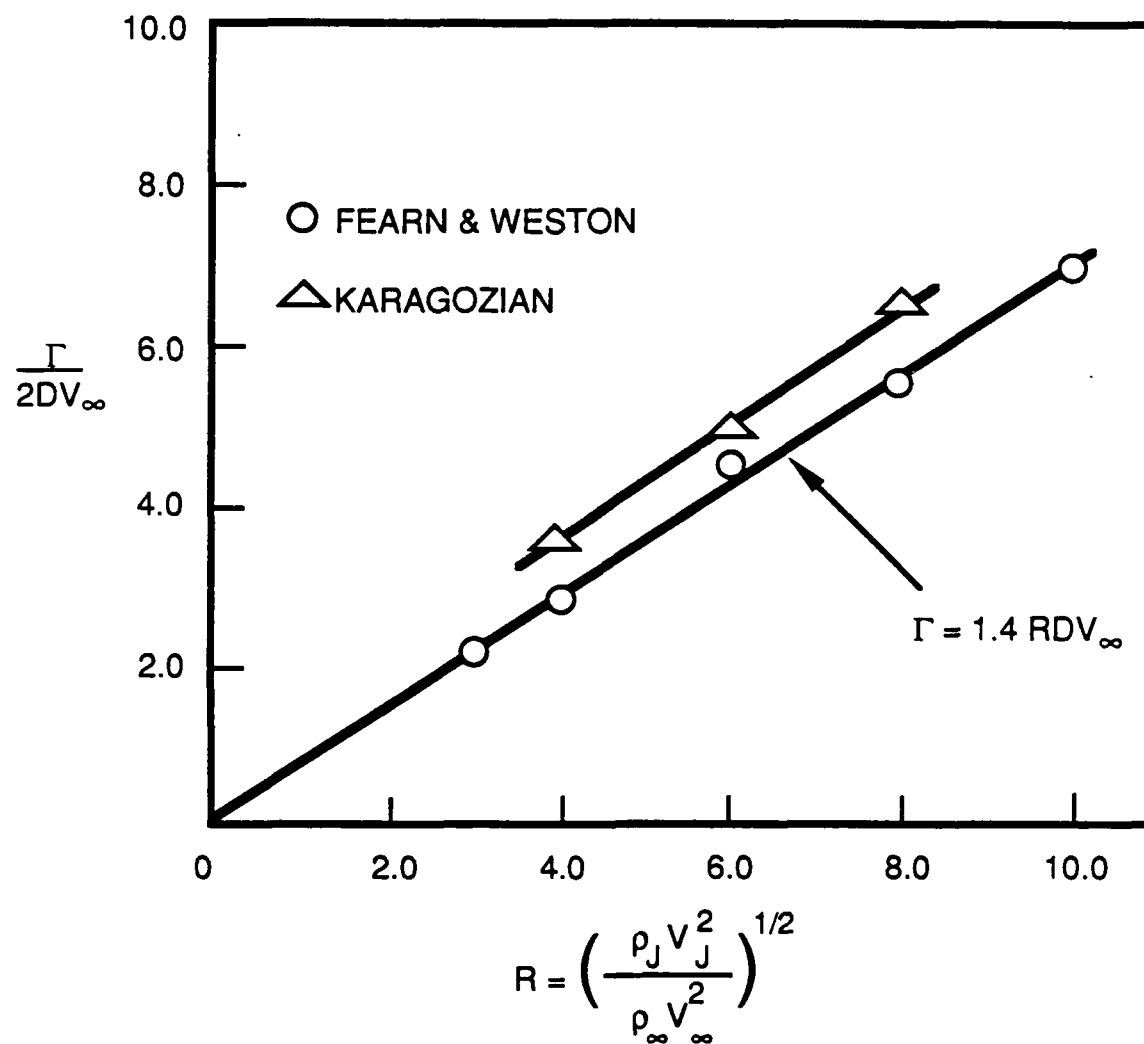
Figure 2.4.   Initial vortex strength for normal injection into subsonic flow.

16

The location of each vortex center is estimated from the jet centerline and vortex center trajectory data of Fearn and Weston (Ref. 4). The general form of the trajectory equation is given by the following expression where the a, b, and c coefficients are different for the jet centerline and vortex center.

$$h/D = aR^b (x/D)^c \tag{2.30}$$

where h is distance from the wall to either the jet centerline or the vortex center. The coefficients are given for the jet centerline as: $a = 0.9772$, $b = 0.9113$, $c = 0.3346$ and for the vortex center as: $a = 0.3473$, $b = 1.127$ and $c = 0.4291$.

The angle of inclination (θ) of the jet centerline to the wall is obtained from the slope of Equation 2.30. At $x = o$, the largest angle is θ_2 (for jet 2, see Fig. 2.2). Thus, for a specified value of θ_2, the corresponding x_2 distance is given by:

$$x_2 = D_2 \left(0.327R^{0.911}/\text{Tan}\theta_2\right)^{1.5} \tag{2.31}$$

The x_1 location is given by:

$$x_1 = x_2 + L \tag{2.32}$$

For a given value of θ_2 (typically 20 deg), Equations 2.31 and 2.32 define x_1/D_1 and x_2/D_2 and Equation 2.30 gives the values of h_1 and h_2 for the vortex center and the jet centerline location at $x = o$.

The distance along the vortex center curve is given by:

$$S = \int_o^x \left[1 + \left(\frac{dh}{dx}\right)^2\right]^{1/2} dx$$

$$\frac{dh}{dx} = 0.149R^{1.127}/(x/D)^{0.571} \tag{2.33}$$

where x_1 defines S_1 and x_2 defines S_2.

17

The vortex half-spacing (d_1, d_2, d_3) of Figure 2.3 is obtained from Figure 7 of Reference 4 and is given in Figure 2.5. The x locations for the data of Figure 2.5 were determined for $\theta_2 = 20$ deg.

The actual jet shape is that of a horseshoe with the jet centerline at the closed end and the vortices located in the legs at the open end. Although there is no intrinsic difficulty in using a fine mesh to resolve the horseshoe geometry, the coding to define the mesh becomes quite complicated and the computational cost is increased significantly. Therefore, the jet geometry has been approximated by an elliptical cross section with the vortex located on the major axis of the ellipse. The actual jet geometry used in the calculation is shown in Figure 2.6 where the elliptical cross section has been truncated into a rectangle to simplify the mesh generation. The unit computational cell in Figure 2.6 corresponds to that shown in Figures 2.1 and 2.2 and contains one-half of a large jet (JET1) and two halves of the small jet (JET2). The jet areas are defined in Appendix B and the location is defined by Equations 2.30 through 2.32. To close the geometry, the ratio of jet major to minor axis (ϵ) must be specified. Experimental data suggest values of ϵ in the range of one to five. However, there are additional constraints on ϵ dictated by the hole spacing and the vortex locations. That is, the extent of the jets in the z direction must be large enough to incorporate the vortices inside the jet and small enough such that the two half-jets do not touch. With these constraints, a value of $\epsilon = 2.0$ seems to be a reasonable choice and this value has been used for all the calculations of this report.

The experimental information given above should provide a reasonable estimate for the initial jet vorticity. However, since the experimental data are for a single pressure matched jet exhausting into an unbounded flow, it is important to emphasize that this is only an estimate. In particular, the symmetry conditions imposed by the injection hole spacing and locations are not present in the experimental data base.
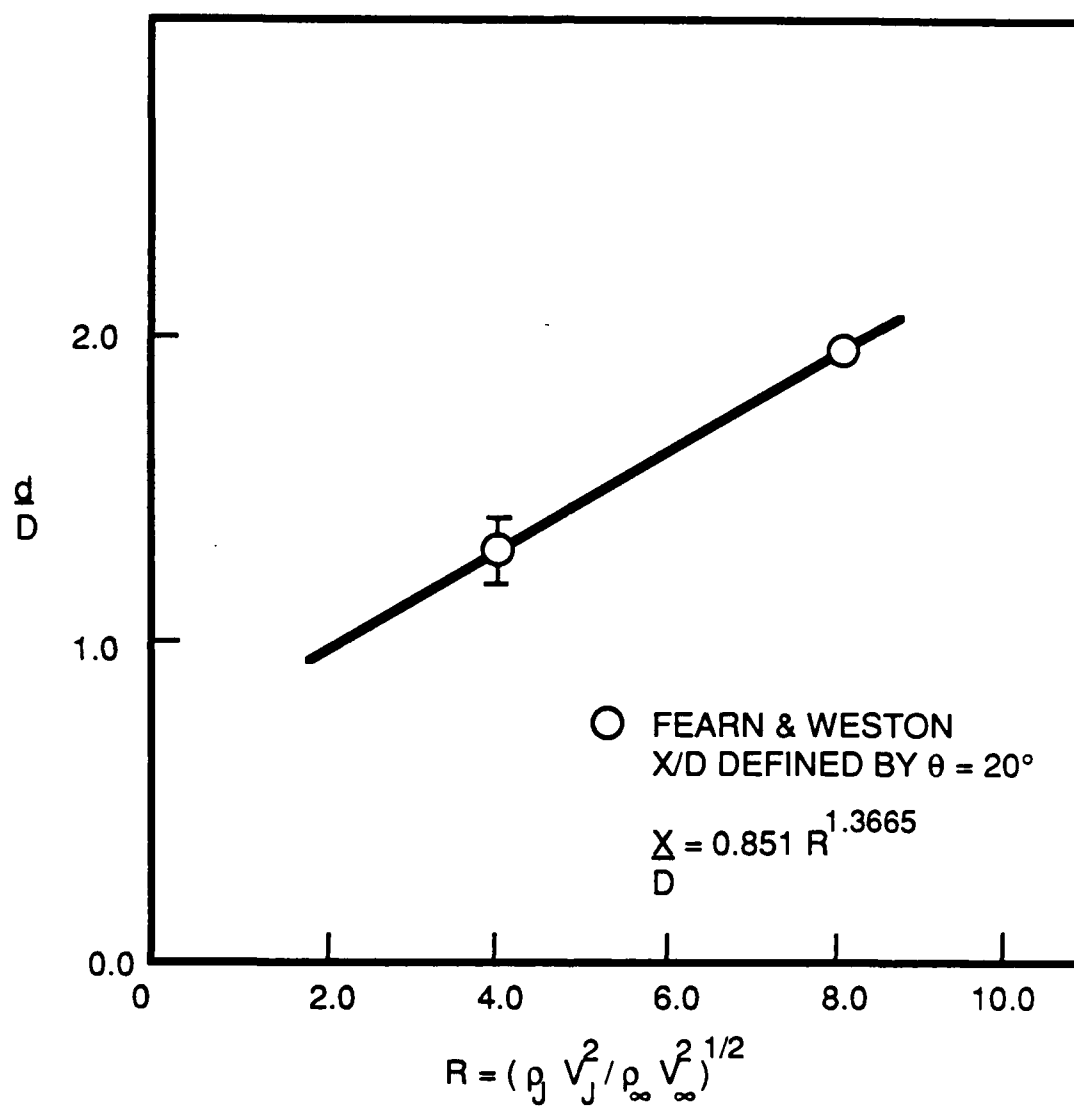
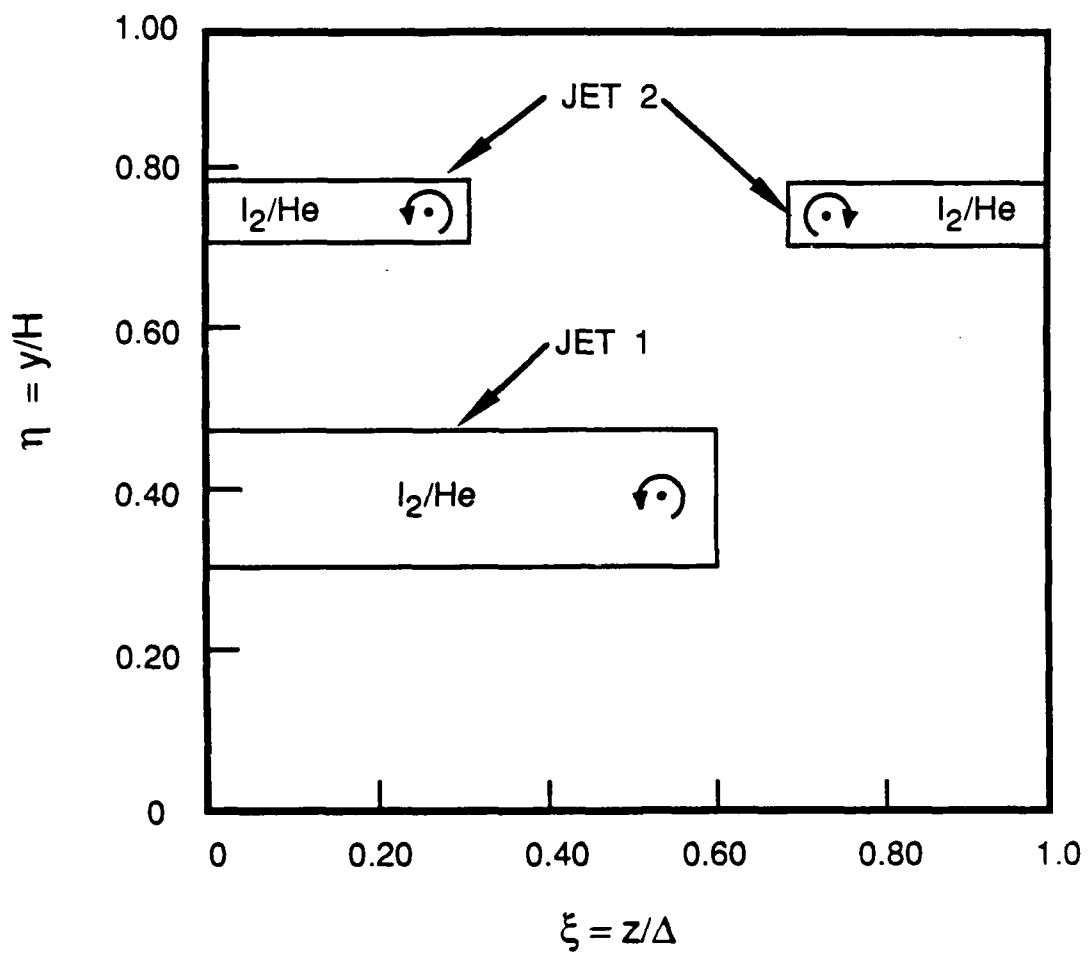Figure 2.5. Vortex half spacing.

Figure 2.6.   Initial jet geometry.

SECTION 3
NUMERICAL ANALYSIS

The equations of Section 2 are defined in terms of the physical coordinates x, y, and z. The actual calculations are carried out in the transformed η and ζ coordinate system. The transformed coordinates are defined by:

$$\eta \equiv y/H(x) \qquad\qquad \zeta \equiv z/\Delta(x) \qquad\qquad (3.1)$$

where a nonuniform cartesian mesh is used in the η-ζ coordinate system.

The equations are differenced using a first-order accurate two-point backward difference for the x derivatives and second-order accurate three-point central difference for the η and ζ differences.

After differencing, all the linearized equations have the following form:

$$AU_{j+1,k} + BU_{j,k} + CU_{j-1,k} + DU_{j,k+1} + EU_{j,k-1} + w\wp = F \quad (3.2)$$

where the coefficients A, B, C, D, E and F are all known functions of j and k. The index j is in the η direction and the k index is in the ζ direction. The term with $\wp$ denotes the pressure gradient in the axial momentum equation (Eq. 2.5) and is not present for the other equations. Therefore, w = -1.0 for the momentum equation and w = o for all the other equations. The variable U is solved for using an implicit formulation where the block tridiagonal approach is used to solve the linear system of equations. An iterative approach is used where the coefficient arrays are updated after each iteration and Equation 3.2 is solved repeatedly until some error criterion is satisfied. Then a new step is taken in the x direction and the process is repeated.

21

When the momentum equation is solved, the pressure gradient $\wp$ is solved simultaneously with the axial velocity by satisfying Equation 2.6 in the form:

$$\phi = \int_0^1 \int_0^1 \theta U \, d\eta d\xi$$

$$\phi \equiv \dot{m}/(H\Delta) \tag{3.3}$$

where θ is a given function and U denotes the axial velocity. For incompressible or low-speed flow where the density varies slowly with pressure, θ is the density ρ evaluated at the previous iterate level. For supersonic flow, where the density varies strongly with pressure, Equation 2.6 is written as:

$$\phi = P \int_0^1 \int_0^1 \theta U \, d\eta d\xi$$

$$\theta \equiv \bar{M}/RT \tag{3.4}$$

where T is the temperature and $\bar{M}$ is the mixture molecular weight. The pressure P is related to the pressure gradient $\wp$ through the use of a backward difference:

$$\wp = (P - P_L)/dx \tag{3.5}$$

where P_L is the pressure at the previous x station.

Thus, for incompressible or subsonic flow, Equations 3.2 and 3.3 are solved simultaneously for U and $\wp$. For supersonic flow, Equations 3.2, 3.4 and 3.5 are solved simultaneously for U, $\wp$ and P.

The solution procedure is to use some quadrature to express the integral of Equation 3.3 or 3.4 as a linear sum which can be solved within the framework of the block tridiagonal approach. This approach was used by Crowell (Ref. 1) and Truman (Ref. 6) for 2-D

22

flows. The extension to 3-D flows is straightforward but tedious and the details are omitted here. The difference between the solution using the subsonic or supersonic formulations is that the supersonic formulation results in a quadratic for the pressure, whereas the subsonic or constant density formulation yields only a single solution branch. The two solution branches obtained from the use of Equation 3.4 are both physically valid and represent subsonic and supersonic solutions. For supersonic flow, the lower pressure is always used. For low subsonic flows, the higher pressure is always used. However, for subsonic flow near Mach 1, the correct pressure can be on either solution branch and some care is required in choosing the correct value.

The solution procedure for Equation 3.2 using the block tridiagonal approach marches in the j direction from J = 1 to J = JMAX and solves a full matrix for the KMAX values of the recursion coefficients at each J value. The solution for U is obtained by back substitution from J = JMAX to J = 1. The computational effort is proportional to JMAX(KMAX)^3. Therefore, it is extremely important to choose the J direction as the direction with the largest number of mesh points. For the case shown in Figures 2.1 through 2.3, the H dimension is nearly four times the Δ dimension and there are about three times as many mesh points in the y direction as in the z direction. Therefore, it is critical that the J dimension be in the y direction. Choosing the J dimension in the z direction would increase computational cost by a factor of 9.

SECTION 4
RESULTS AND DISCUSSION

The case of most interest to WL/ARDI is the modeling of the flow in the RotoCOIL device where the iodine injection takes place in a subsonic channel and the flow is expanded through a throat to achieve supersonic cavity flow. In principle, the TRIMIX code can model this flow geometry by iterating upon the upstream pressure until sonic flow in the throat is achieved. However, this constitutes a classical problem in fluid dynamics where a saddle point singularity exists at Mach 1 and can only be integrated with great difficulty, using a marching technique. The practical difficulty is that the solution must be extremely accurate to integrate smoothly through the throat. This translates into a requirement that the initial pressure must be iterated until it is known to within a tolerance of 0.01 torr. Typically, this would take 10 or 12 iterations, each one of which would consume 3 to 4 h of computer (CRAY 1) time. Although the solution obtained in this manner is exact, it is computationally expensive. One way around this problem is to specify the pressure distribution and accept the associated error in the global mass flux. That is, if P is specified in the momentum equation, then there is no way to ensure that Equation 2.6 is satisfied. That is, an error in pressure will result in an error in the global mass flux. Therefore, to limit the mass flux error to some acceptable level, a reasonably accurate pressure distribution must be supplied to the calculation. Since the pressure is determined primarily by the area schedule and the loss in momentum due to wall shear, it seems plausible to assume that a one-dimensional (1-D) premixed calculation could be used to obtain the pressure distribution. The 1-D premixed calculation must also iterate on the initial pressure to achieve sonic flow at the throat but the computational cost of this calculation is less than a half-hour of CRAY 1 time. This approach has been used with the 2-D JETMIX code for mixing calculations and has worked quite well, with the error in mass flux oscillating between 5 and 10 percent over all the streamwise locations. Since the mass flux

24

error is distributed over all the species, it is believed that the error in the species mass fractions is less than the error in the global mass flux. This approach should also work for the 3-D mixing problem and therefore the TRIMIX code contains an option to either calculate the pressure by satisfying global continuity or specify the pressure.

Since it is believed that most of the mixing and I_2 dissociation takes place in the subsonic flow upstream of the throat, the calculations will concentrate on this region. To avoid the pressure iteration described above, the throat is removed and the calculations are done for a constant area channel where the initial conditions are those of the RotoCOIL nominal operating point. The conditions upstream of the iodine injection and the geometry are given as:

$$
\begin{aligned}
P &= 34.71 \text{ torr} \\
T &= 275 \text{ K} \\
Y &= 0.37 \\
U &= 0.93 \\
P(H_2O) &= 0.897 \text{ torr} \\
\dot{x}(He) &= 4.54 \text{ moles/s} \\
\dot{x}(O_2) &= 1.385 \\
\dot{x}(Cl_2) &= 0.107 \\
\dot{x}(H_2O) &= 0.16 \\
\dot{m} &= 0.023186 \text{ g/s} \\
H &= 0.37338 \text{ cm} \\
\Delta &= 0.09726 \text{ cm}
\end{aligned}
\tag{4.1}
$$

Note that the molar flow rates are those for the entire nozzle bank whereas the mass flux ($\dot{m}$) is for the unit computational cell defined by H and Δ. The I_2/O_2 molar flow ratio is 0.01487 and the injected molar ratio of He/I_2 is 43.835. It is assumed that the

injected flow is choked at the orifice hole to give a value of the square root of the momentum ratio of R $\dashv$ 2.763. The injected I_2 and He has a total temperature of 366 K. The corresponding information from Section 2.3 is given as:

$$\Gamma/DV_\bullet = 3.87$$
$$\eta_1 = 0.3865$$
$$\eta_2 = 0.747$$
$$\zeta_{p}1 = 0.2612$$
$$\zeta_{p}2 = 0.5223 \qquad\qquad (4.2)$$

where the η coordinates are the jet centerline locations for the indicated jets and the ζ_p coordinates are the vortex center locations (see Figs. 2.3 and 2.6). The initial jet and vortex locations are shown in the transformed plane in Figure 2.6. For all the calculations of this report, 10 species (I_2, He, I, I_2^*, I^*, H_2O, $O_2(^1\Delta)$, $O_2(^1\Sigma)$, $O_2(^3\Sigma)$, Cl_2) and the 21 reactions of the reduced WL oxygen/iodine kinetics package (Table 2.1-VI of Ref. 7) were used.

The calculations used 48 mesh points in the η direction and 16 mesh points in the ζ direction. The step size in the x direction started at 0.01 cm and was ramped up to 0.03 cm. The calculation was run out to 1.8 cm and a total of 66 steps were taken in the x direction. The computation time was 3.89 h on the CRAY 1 machine.

The initial distribution for the axial vorticity and the velocity components are contained in Figure 4.1. Note that the vorticity is large enough to induce secondary flow velocities of the same magnitude as the axial velocity. The convection and diffusion of the iodine jet can be seen in Figure 4.2 with increasing distance from the initial x location. The buildup of the gain is shown in Figure 4.3. The profiles at the x = 1.8 cm station are contained in Figure 4.4.
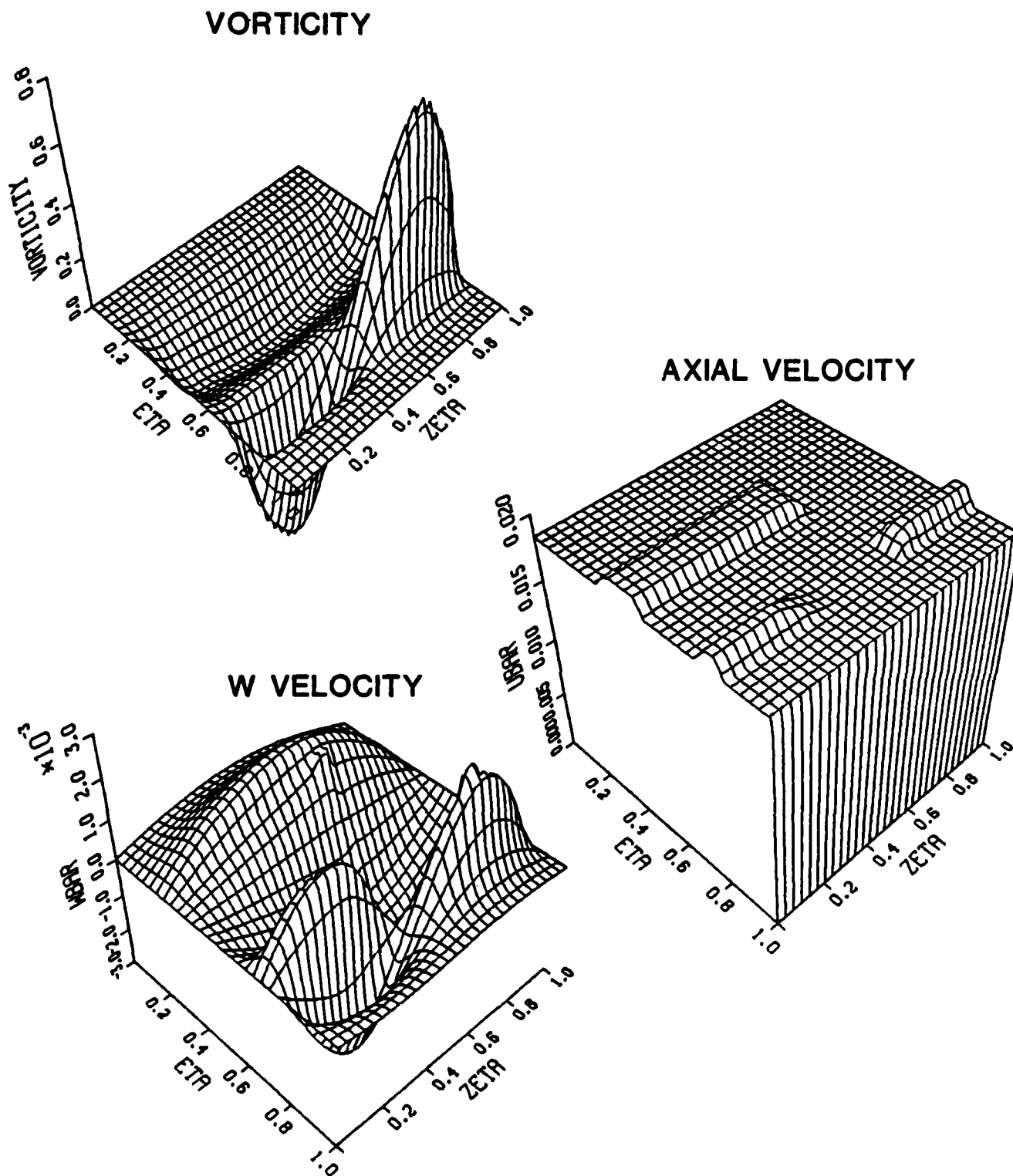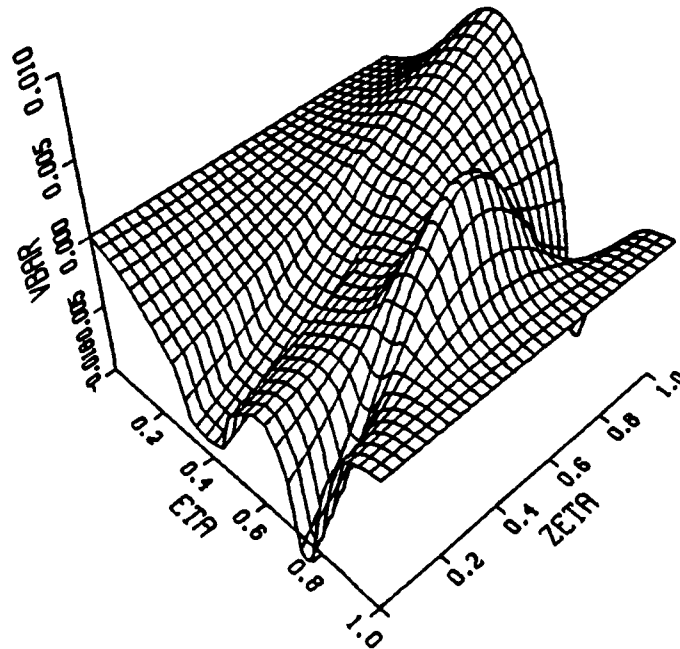
26

VORTICITY

AXIAL VELOCITY

W VELOCITY

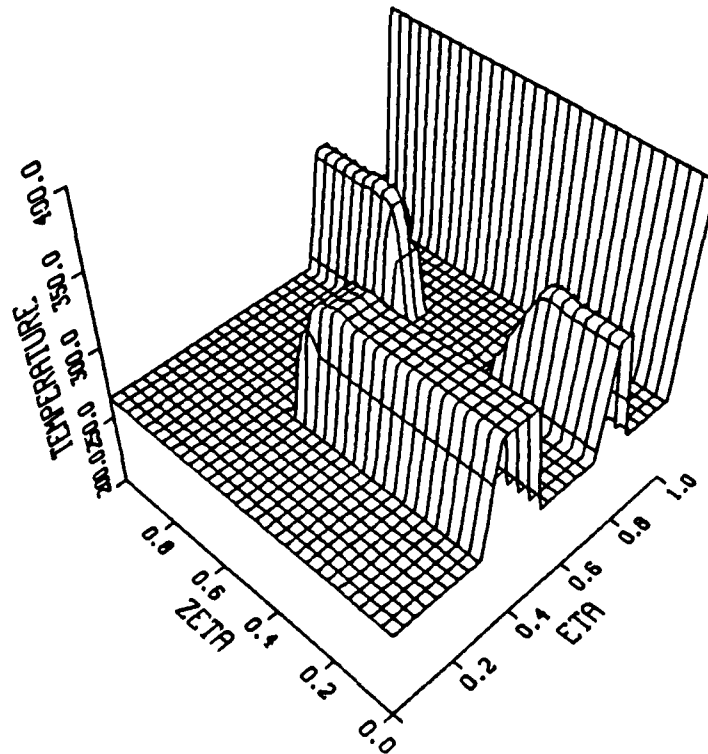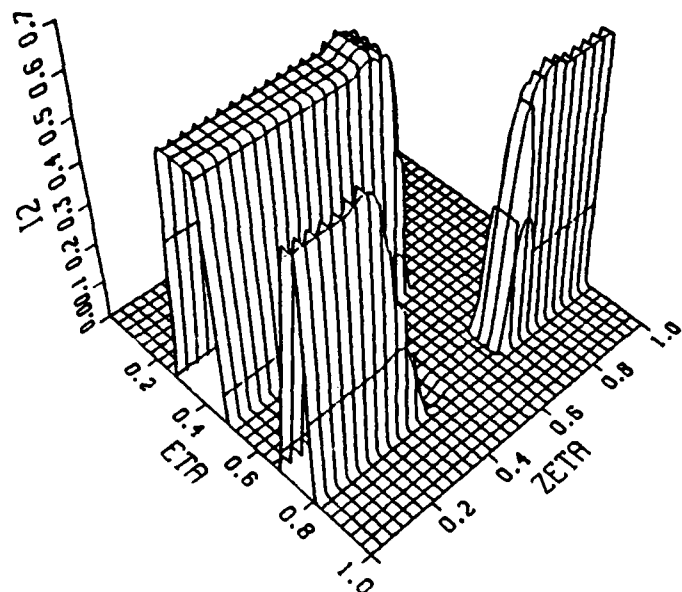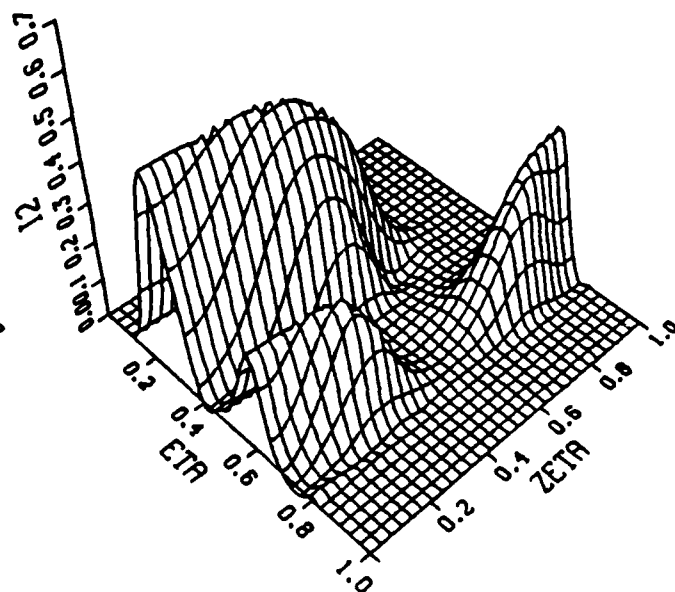Figure 4.1.   Initial distributions at x = 0.

V VELOCITY

TEMPERATURE

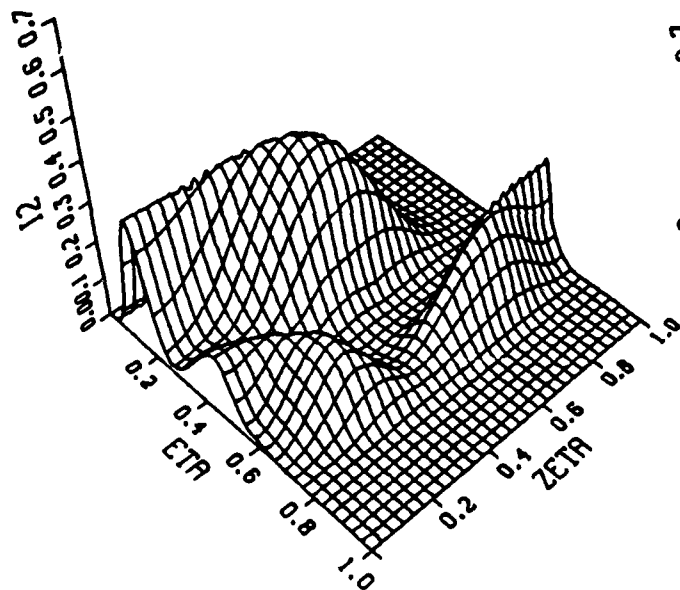Figure 4.1. Initial distributions at x = 0 (Continued).

X = 0.000 cm   X = 0.209 cm

X = 0.509 cm   X = 0.809 cm

Figure 4.2.   I$_2$ concentration versus flow distance.
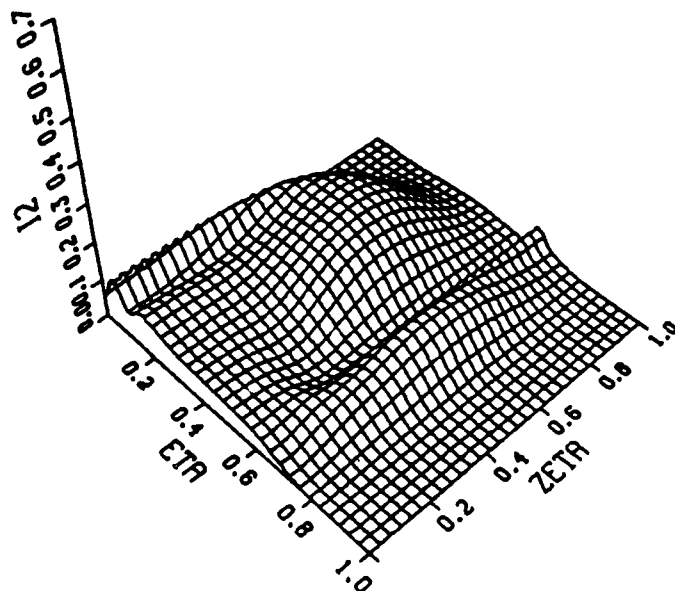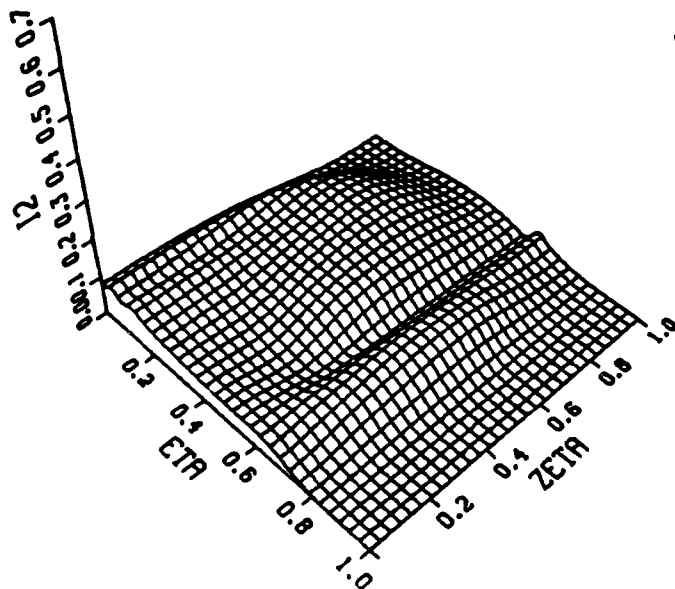
29
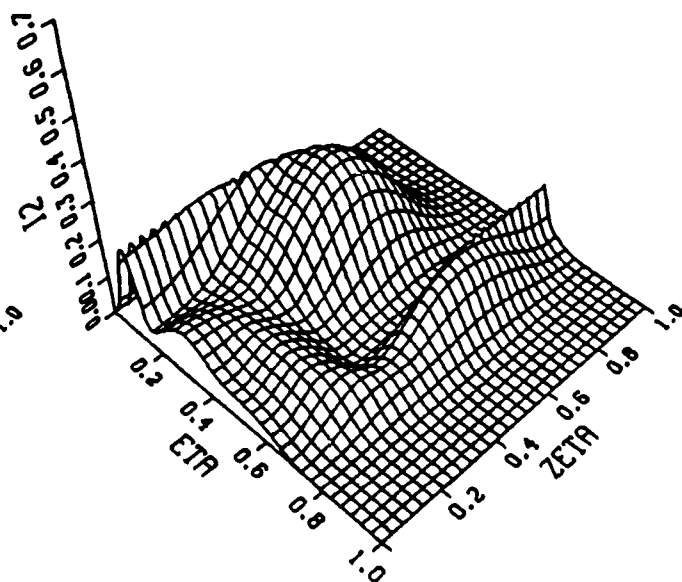
X = 1.009 cm
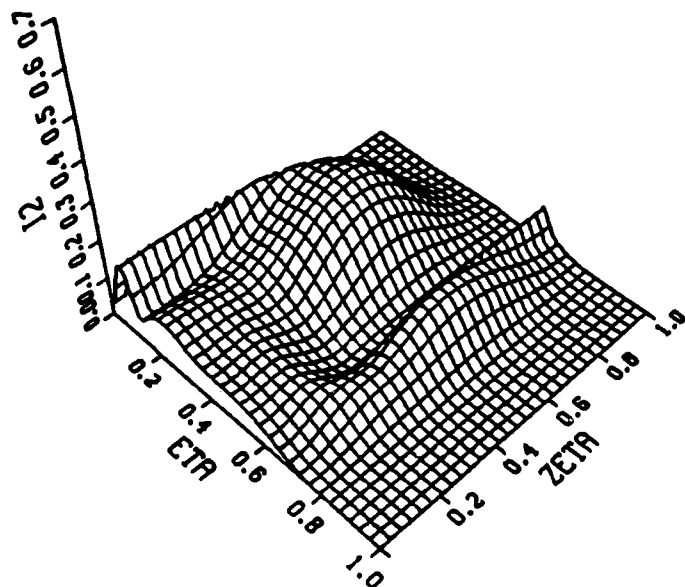
X = 1.209 cm

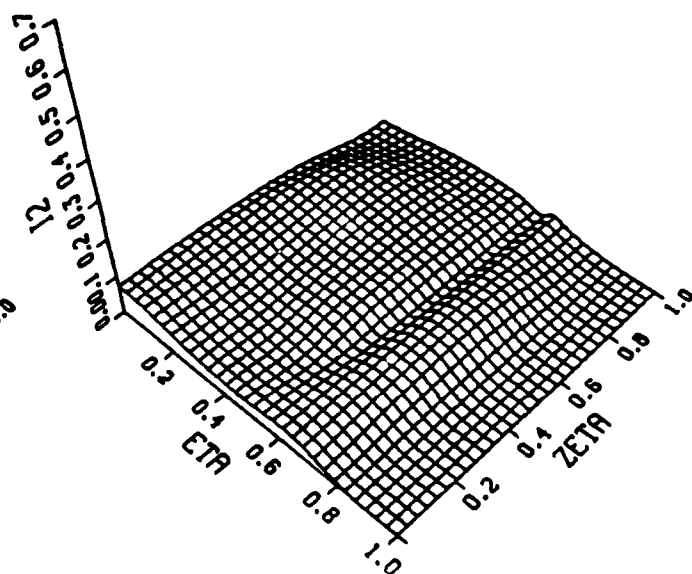## X = 1.509 cm

X = 1.809 cm

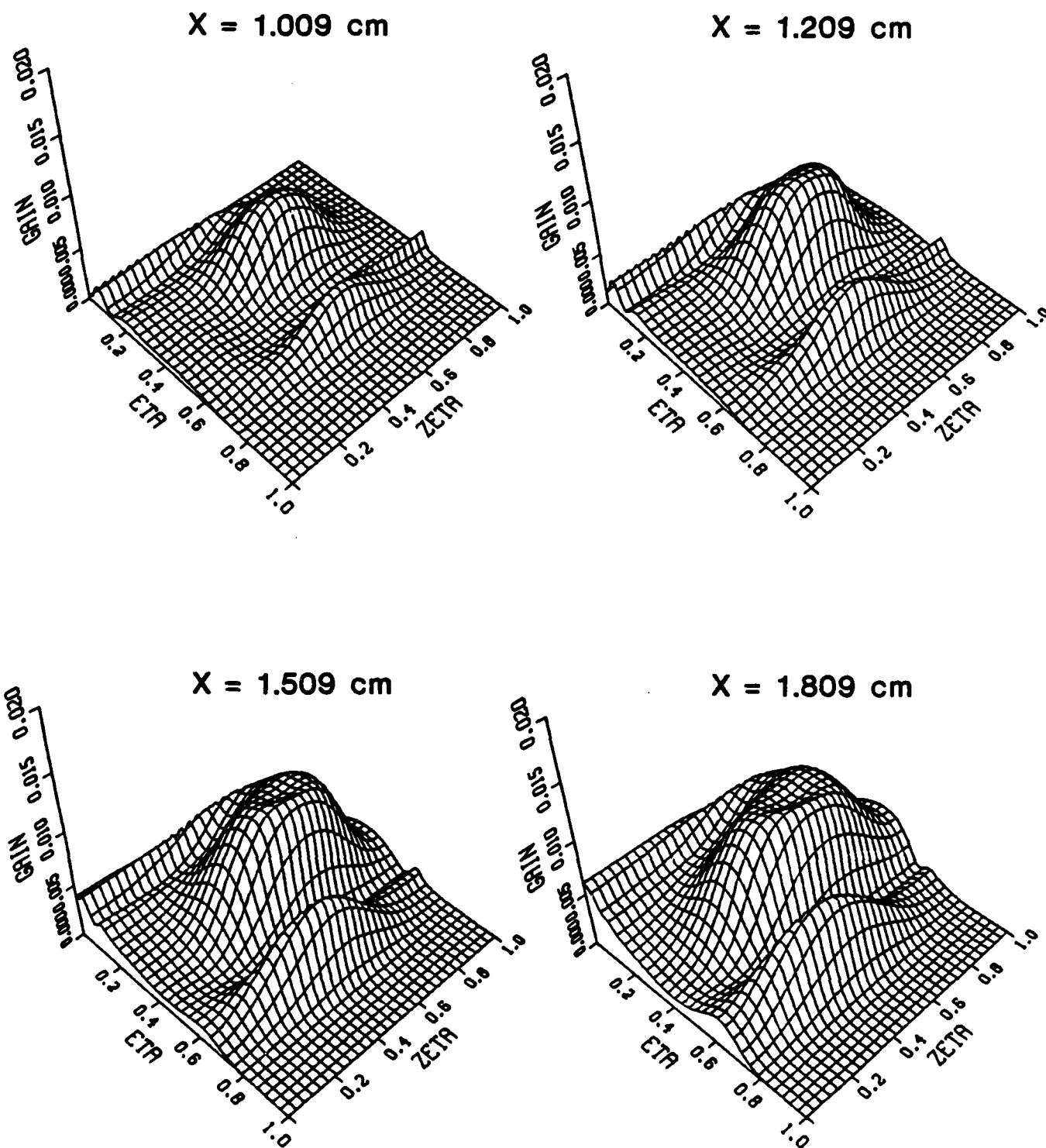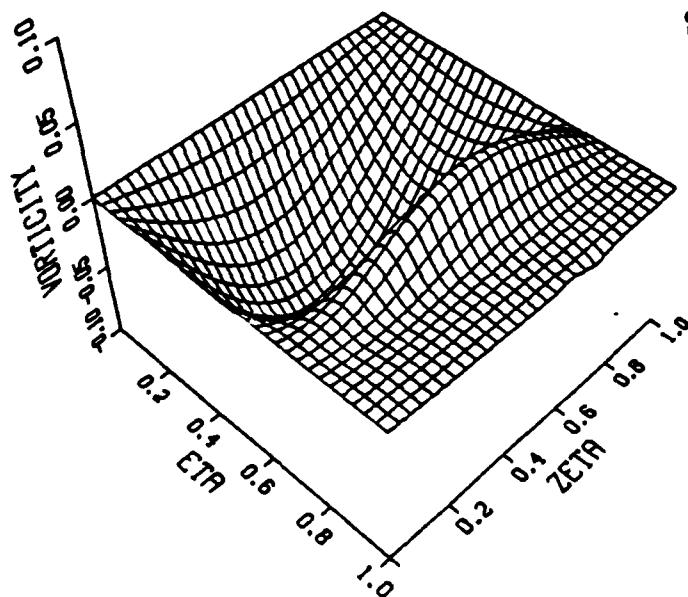Figure 4.2. I_2 concentration versus flow distance (Continued).

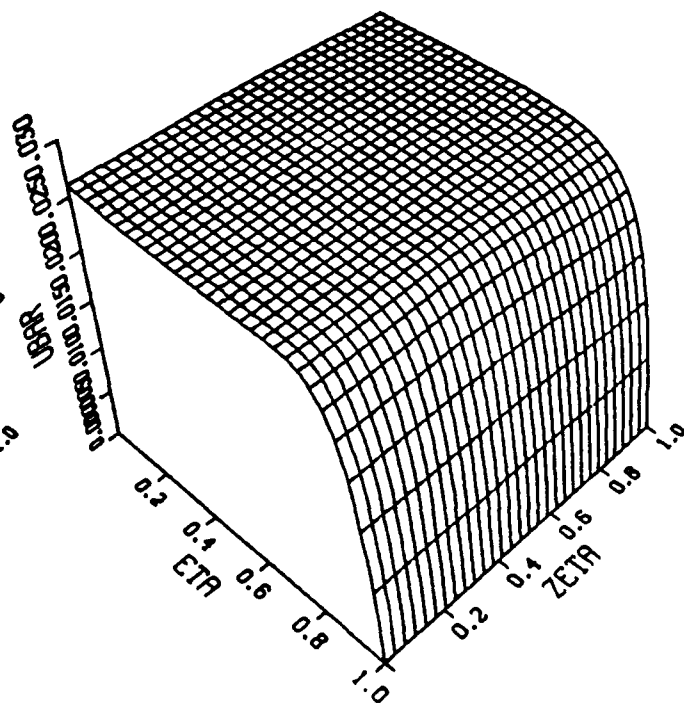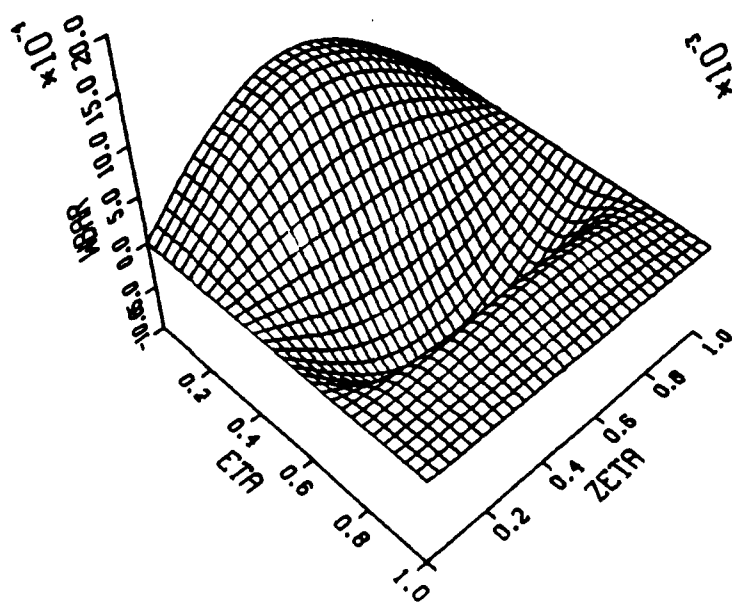Figure 4.3. Gain distribution versus flow distance.

VORTICITY MAP
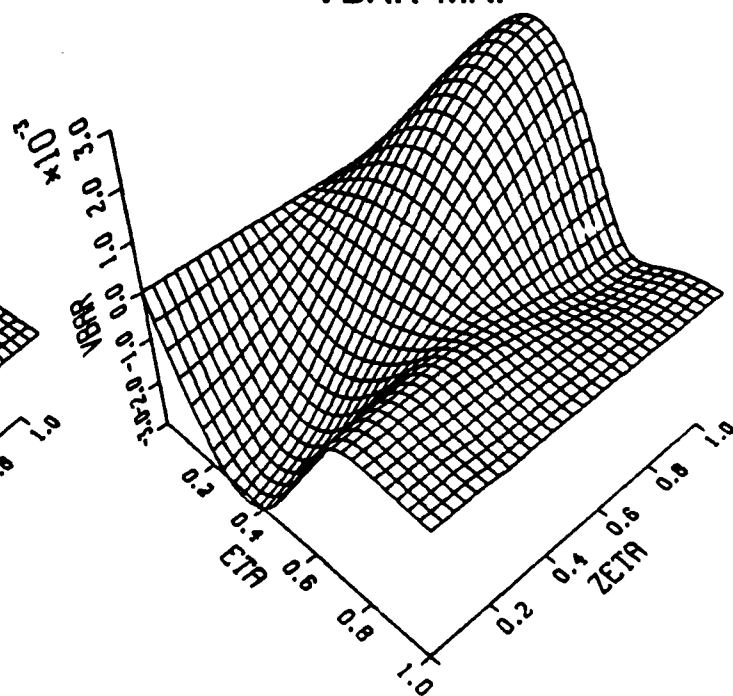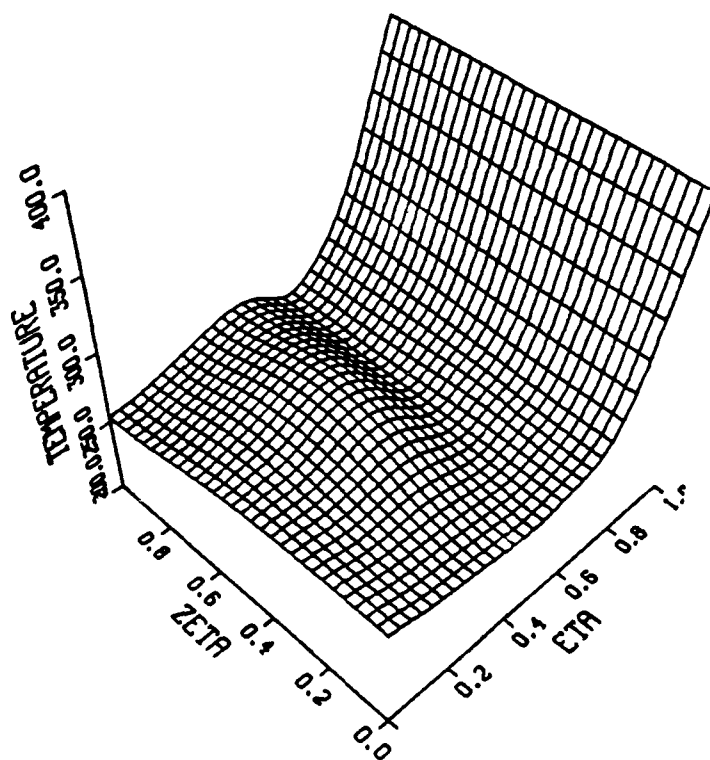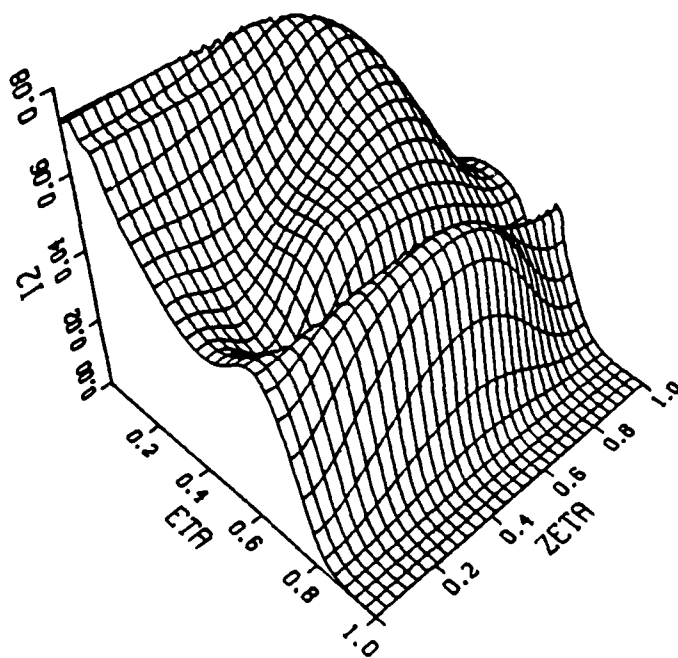
UBAR MAP

WBAR MAP

VBAR MAP

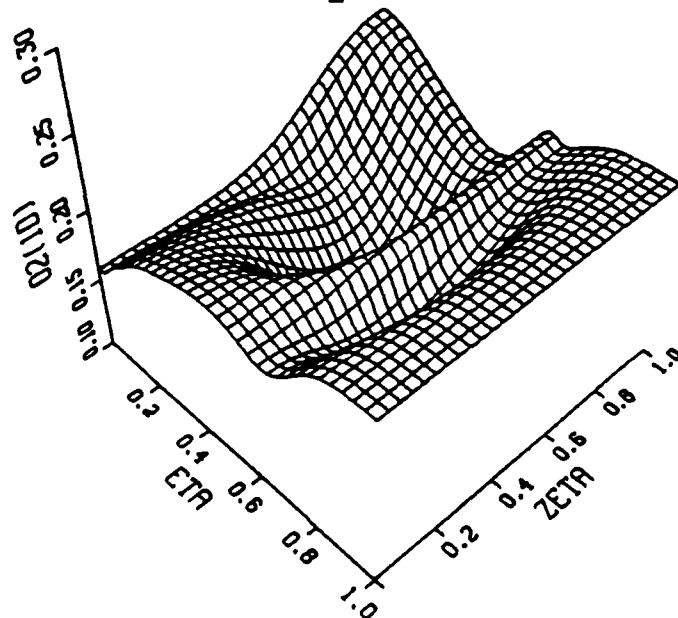Figure 4.4.   Distributions at x = 1.809 cm.

32

TEMPERATURE MAP

I2 MAP

O$_2^{1\Delta}$ MAP

I* MAP
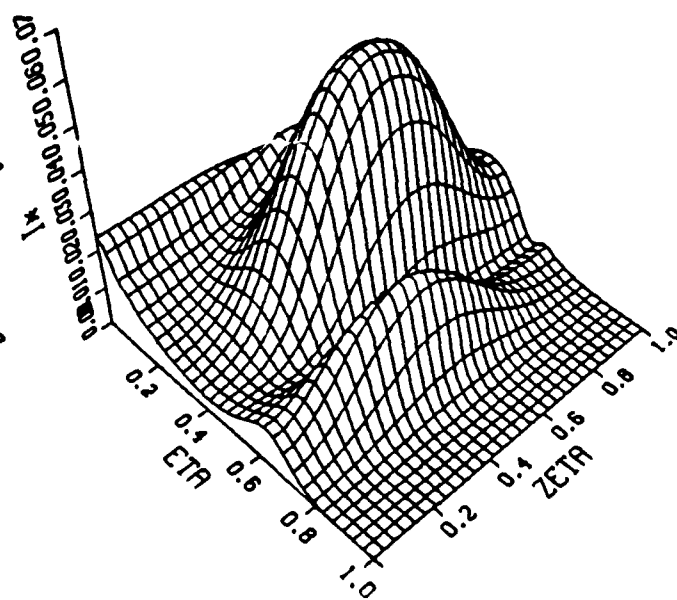
Figure 4.4.   Distributions at x = 1.809 cm (Continued).

33

4.1 COMPARISON OF 3-D MIXING AND 1-D PREMIXED CALCULATIONS.

The premixed assumption is frequently used to carry out performance calculations for COIL laser devices (see Ref. 8 for example). In this manner, the mixing calculation is eliminated by assuming instantaneous mixing between the primary and secondary flows. This reduces the 3-D chemically reacting flow problem to a 1-D problem with a corresponding reduction in computer cost by a factor of 100. The TRIMIX code contains an option to premix the reactants at the initial station and carry out the premixed calculation to provide a comparison between the premixed assumption and the exact 3-D results. To compare the results, average values are defined for the gain and species as follows:

$$\overline{K}_i \equiv \frac{H\Delta}{\dot{m}} \int_0^1 \int_0^1 \rho U K_i \, d\eta d\xi$$

$$\overline{\alpha} \equiv \int_0^1 \int_0^1 \alpha \, d\eta d\xi$$

$$F \equiv 1 - \overline{K}_{I_2} \Big/ \left(\overline{K}_{I_2}\right)_{x=0} \tag{4.3}$$

where K_i and α are the species mass fractions and gain and F is the fraction of molecular iodine which has been dissociated. The bar superscript denotes values which are averaged over the entire computational domain at each x station. The average gain in the direction of the optical axis (y-direction) determines the radiative flux and is defined by:

$$\alpha(\xi)_{opt} \equiv \int_0^1 \alpha(\xi, \eta) \, d\eta \tag{4.4}$$

where the gain calculation is described in Appendix C.

The comparison is contained in Figures 4.5 and 4.6. Figure 4.5 shows the fraction of I_2 dissociated (F of Eq. 4.3) and the average gain ($\overline{\alpha}$) as a function of flow distance and Figure 2.12 shows the optical axis gain (Eq. 4.3). The premixed assumption drastically underpredicts both the amount of iodine dissociation and the small signal gain. To the author's knowledge, this is the first comparison of the premixed assumption with an exact 3-D mixing calculation for an oxygen/iodine laser.

The opinion is often expressed that while the premixed calculation is not exact, it does provide the upper bound (i.e., most optimistic) laser performance. The results of Figures 4.5 and 4.6 clearly dispute this assertion. In this case, the premixed assumption substantially underpredicts the performance. This difficulty with the premixed assumption has been realized for some time (see the discussion on pages 25-28 of Ref. 8). The approach used in Reference 8 to overcome this limitation was to artificially increase the rate constant for the I_2^* formation reaction. That is, the first step in the I_2 dissociation chain is the following reaction.

$$I_2 + O_2(^1\Delta) \xrightarrow{\text{K}} I_2^* + O_2(^3\Sigma)$$

$$K = 7.0 \times 10^{-15} \text{ cm}^3/\text{molecule-s} \tag{4.5}$$
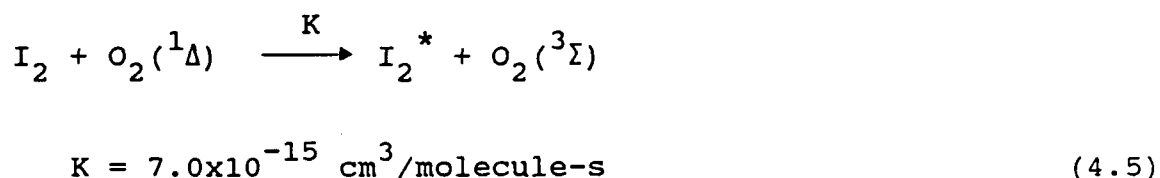
where the indicated rate is the "standard" value from Reference 7. Both the 3-D mixing calculation and the premixed calculations of Figures 4.5 and 4.6 used the rate constant of Equation 4.5.

If the I_2 dissociation fraction is known at some x location, then the rate constant of Equation 4.5 can be chosen to reproduce the known dissociation. From the 3-D calculation, the dissociation fraction is seen to be about 44 percent at x = 1.83 cm. By increasing the rate constant of Equation 4.5 by a factor of 5, the premixed calculation will yield the same result at x = 1.83 cm.

35
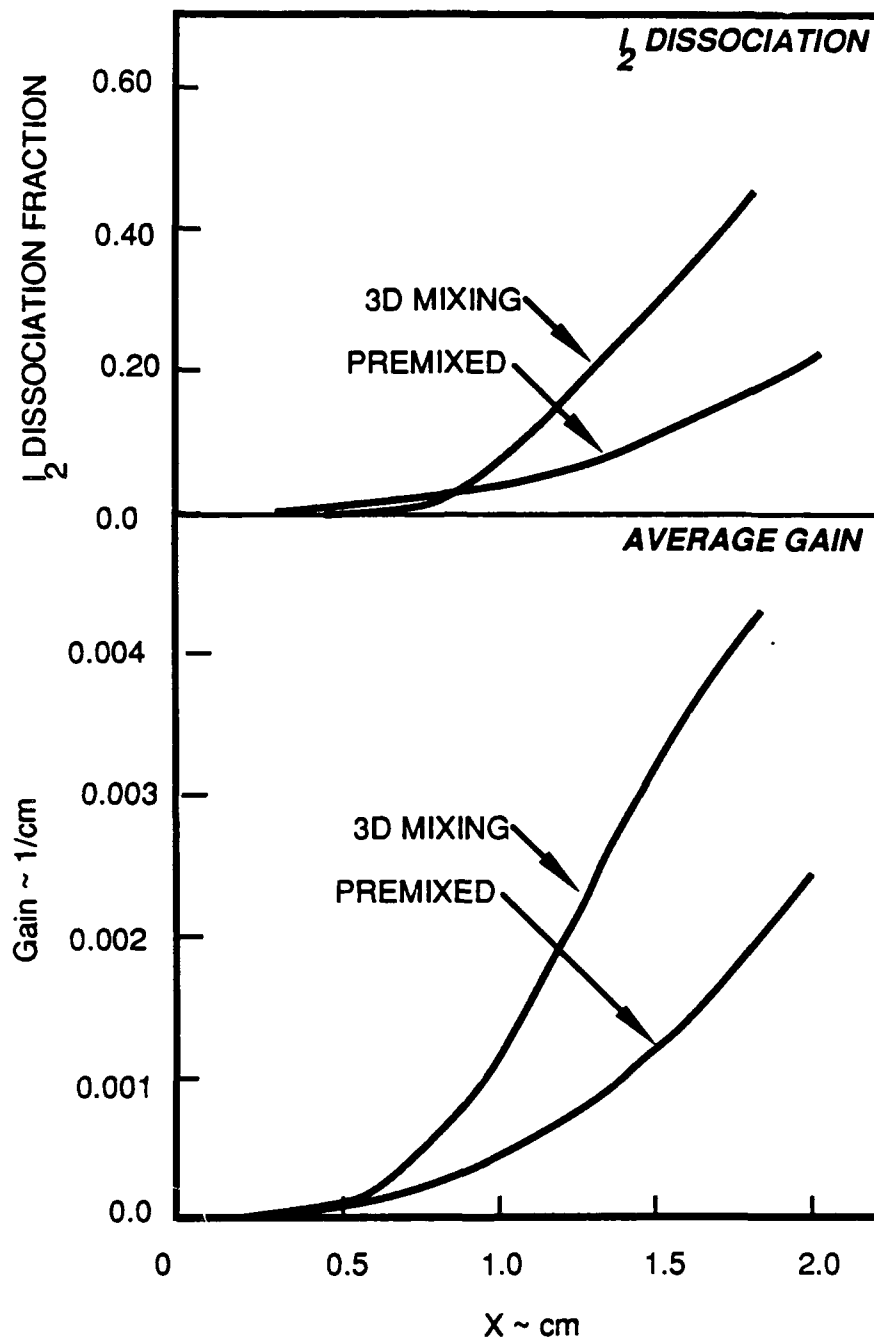
Figure 4.5.   Comparison of 3-D mixing and 1-D premixed
calculations for I_2 dissociation and average gain.
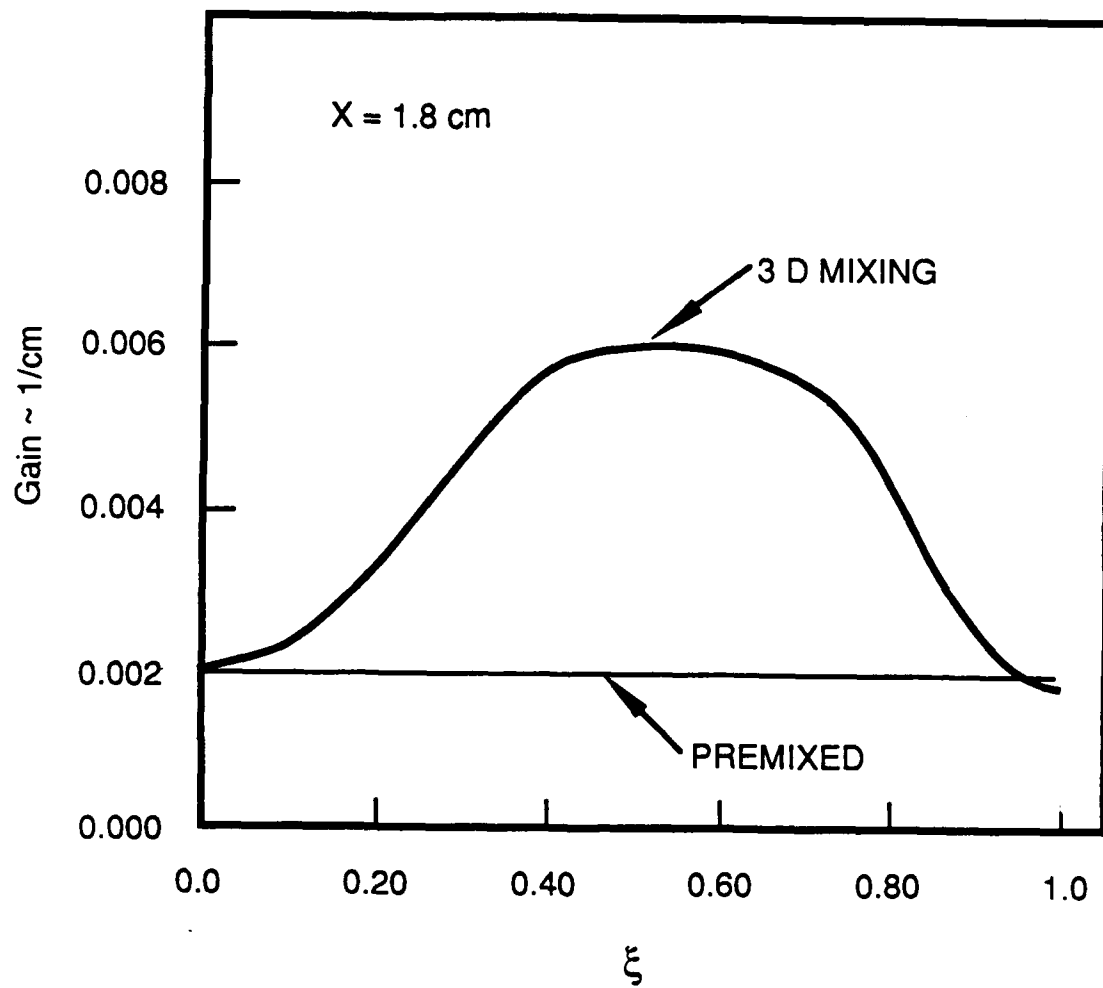
36

Figure 4.6.   Comparison of 3-D mixing and 1-D premixed
              calculations for optical axis gain.

37

This is shown in Figure 4.7. The corresponding small signal gain and yield are compared with the average values from the 3-D calculation in Figure 4.8, and the agreement is quite good. In other words, if the rate constant of Equation 4.5 is increased to reproduce the known level of I_2 dissociation, then the premixed calculation will give the correct average gain and yield. The comparison of Figures 4.7 and 4.8 seems to provide the justification for the use of the premixed approximation with the approach of Reference 8.

4.2 COMPARISON OF DIFFUSION MODELS.

The binary diffusion model (Eq. 2.13) is frequently used in mixing calculations because of its simplicity. One of the objectives of this report was to make a comparison between the binary diffusion and "effective" binary diffusion (Eq. 2.11) models. This comparison is contained in Figures 4.9 and 4.10. In Figure 4.9, the iodine dissociation and optical axis gain are given for the two models where a Schmidt number of unity has been used in the binary diffusion model. These are significant differences between the two models, particularly with respect to the iodine dissociation fraction. The gains profiles at $x = 1.8$ cm are contained in Figure 4.10, which shows that the profile for the binary diffusion model is much smoother than the result for the "effective" binary diffusion model.

Although the differences between the two models are not as great as those reported in Reference 1, they are still sufficiently large to preclude the use of the binary diffusion model. There undoubtedly exists some value of the Schmidt number which would result in closer agreement between the two models. The difficulty is that the "correct" value is not known a priori. The use of the effective binary diffusion model imposed only a 5 percent computational penalty for the calculations of Figures 4.9 and 4.10.

$$I_2 + O_2^{1\Delta} \xrightarrow{k} I_2^* + O_2^{3\Sigma}$$

PREMIXED CALCULATION
$K = 3.5 \times 10^{-14}$

3D MIXING
$K = 7.0 \times 10^{-15}$
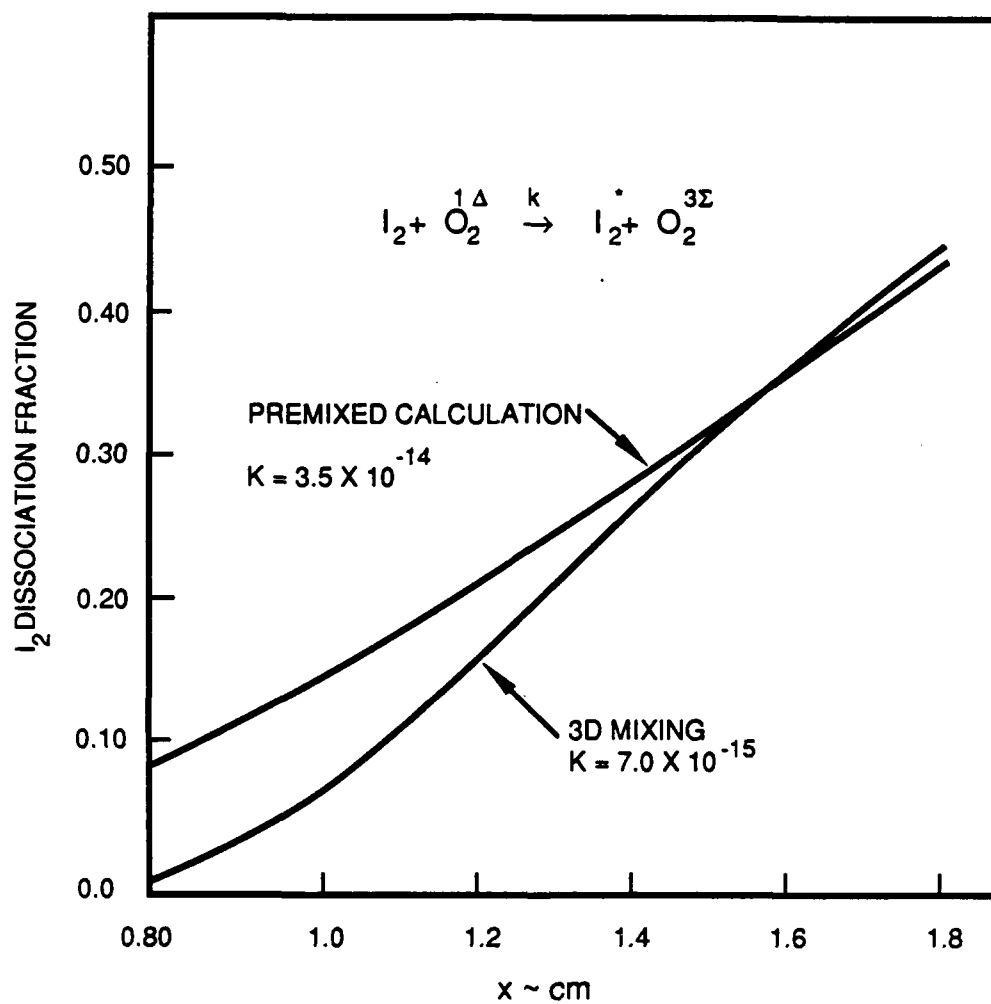
Figure 4.7. Influence of I_2^* formation rate on iodine dissociation.

0.40

YIELD

3D MIXING
K = 7.0 X 10^{-15}

0.35

O PREMIXED
K = 3.5 X 10^{-14}

0.30

0.005

0.004

$$I_2 + O_2^{1\Delta} \xrightarrow{k} I_2^* + O_2^{3\Sigma}$$

GAIN ~ 1/cm

0.003

PREMIXED
K = 3.5 X 10^{-14}

0.002

3D MIXING
K = 7.0 X 10^{-15}

0.001

0.0   0.5   1.0   1.5   2.0

X ~ cm
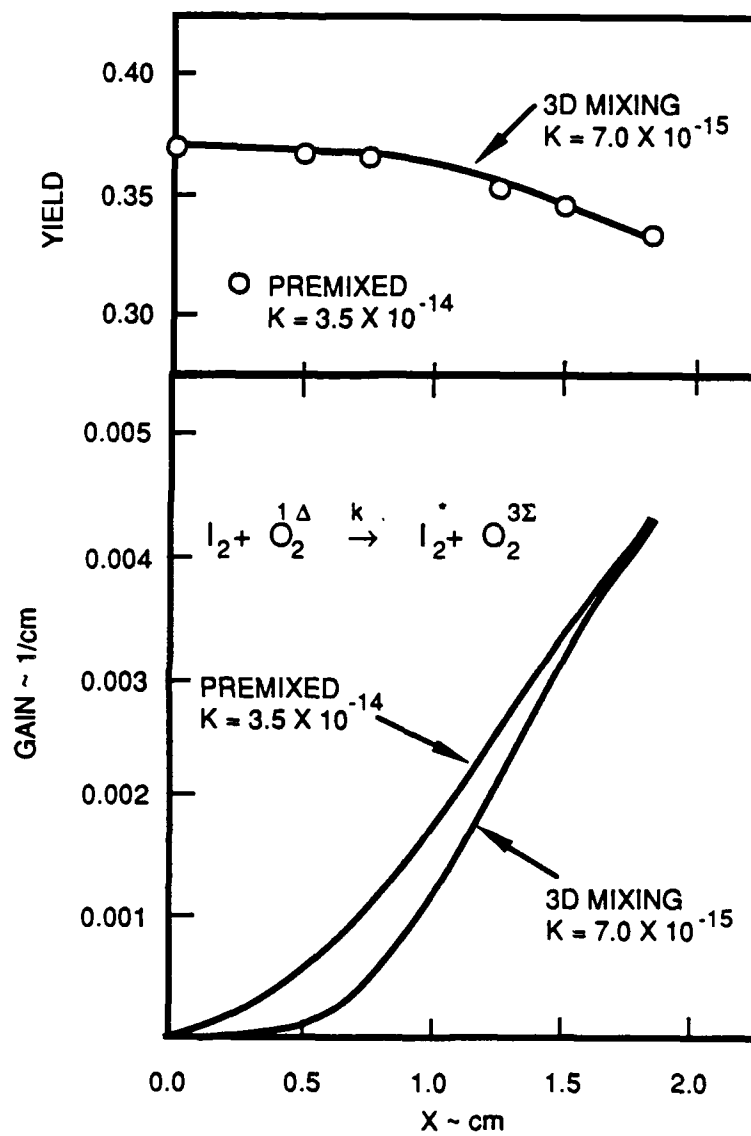
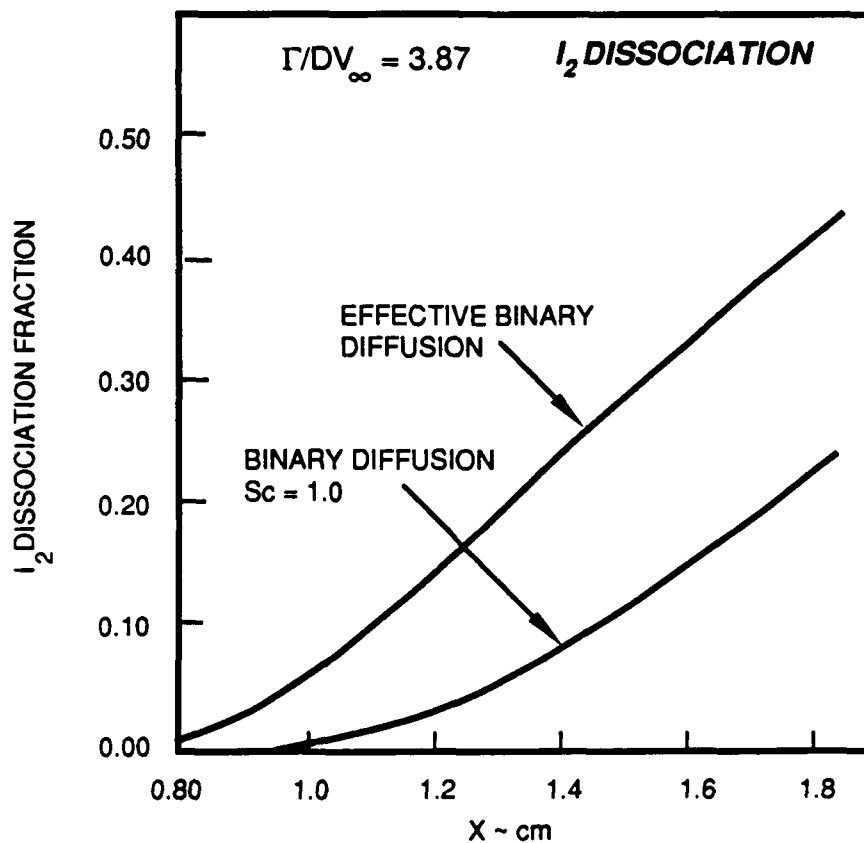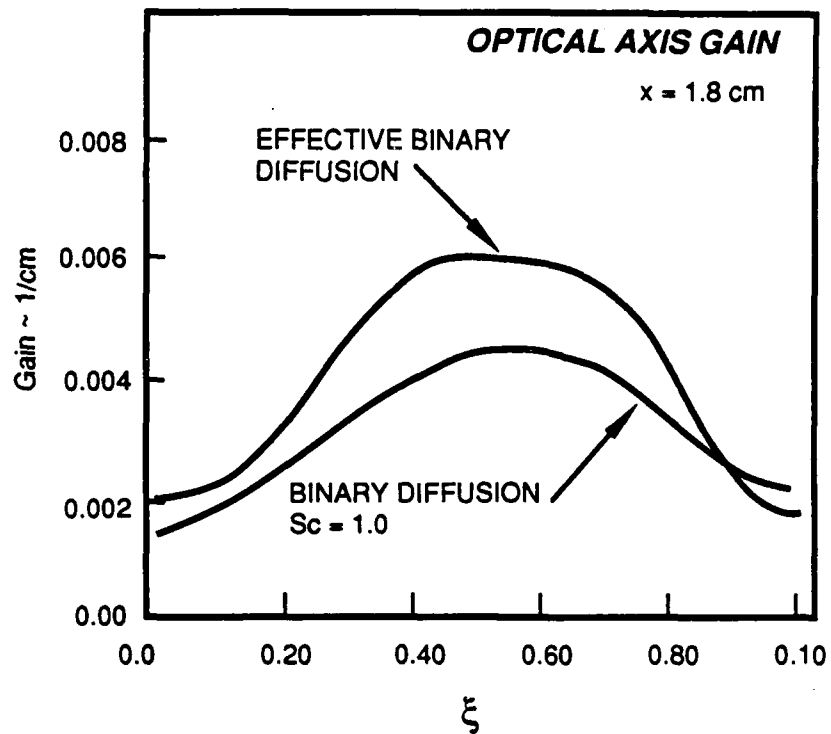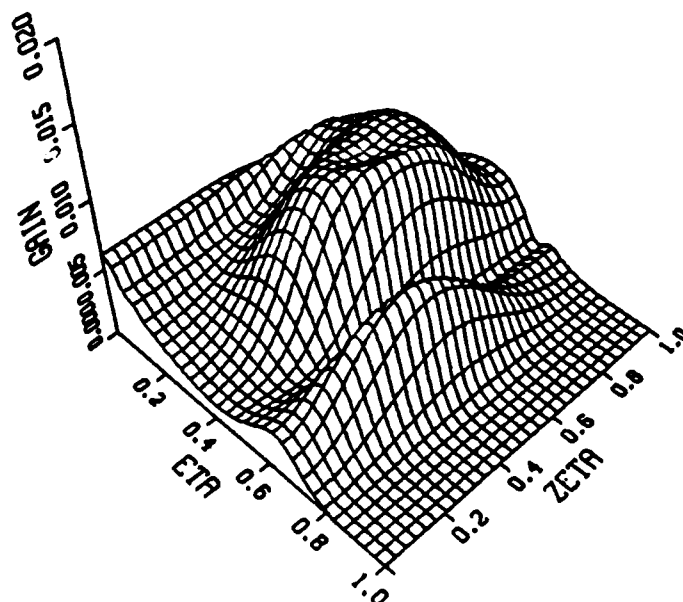Figure 4.8.   Influence of I_2^* formation rate on gain and yield.

Figure 4.9. Influence of diffusion model on gain and iodine dissociation.

EFFECTIVE BINARY DIFFUSION

BINARY DIFFUSION Sc = 1.0

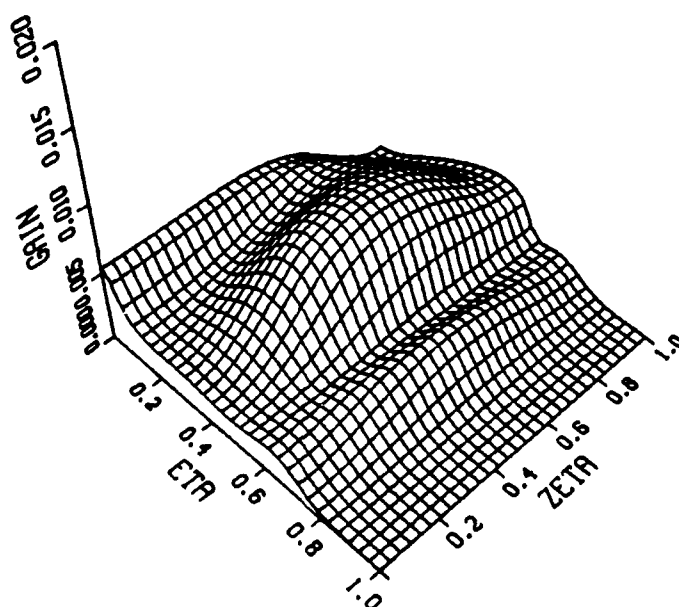
Figure 4.10.   Influence of diffusion model on gain (x = 1.80 cm).

Since the computational penalty is small and there is no ambiguity associated with choosing a value of the Schmidt number, it is recommended that the "effective" binary diffusion model be used in 3-D mixing calculations.

4.3 SENSITIVITY OF RESULTS TO UNCERTAINTIES IN INITIAL CONDITIONS.

As indicated in Section 2.3, the experimental data base upon which the initial conditions are based is for a single jet issuing into an unbounded flow. Since the flow geometry for the present problem consists of multiple jets being injected into a finite flow, the initial conditions of Section 2.3 should be viewed as a reasonable approximation rather than as an exact description of the flow at x = o. In order to assess the impact of uncertainties in the initial conditions upon the computed results, the parameters of Section 2.3 are varied over a plausible range and the calculations are compared with the nominal case.

The β coefficients of Equation 2.25 determine the peak value and the spread of the vorticity. As β increases, for a fixed value of the vortex strength Γ, the peak vorticity increases and the vorticity is more concentrated about the vortex center. The β coefficients are defined in terms of the vortex core size in Equations 2.27 and 2.28. If the vortex core radius was actually half the value given by Equation 2.28, the β coefficients would be four times as large as the nominal values and the peak vorticity would also be increased by a factor of 4. The computed results for this case are denoted by the circle symbols in Figure 4.11. It is seen that this large variation in β has only a minor impact on the gain and I_2 dissociation.

There is also some uncertainty in the vortex half-spacing (the d coefficients of Fig. 2.3) given by Figure 2.5. The nominal values (given by ζ_{p1} and ζ_{p2} of Eq. 4.2) are reduced to move the vortex locations closer to the center of the jet. The nominal vortex centers are shown in Figure 2.6. Moving the vortex center to the

43

midpoints of the jets gives $\xi_{p1} = 0.15625$ and $\xi_{p2} = 0.3125$. The calculated results for this variation are denoted by the triangle symbols in Figure 4.11. The influence on the results is seen to be negligible.

The variation on the vortex strength is contained in Figure 4.12 where the nominal value ($\Gamma/DV_\bullet = 3.87$) has been approximately doubled and halved. The influence on the gain is fairly small as is the influence on I_2 dissociation for the lower value. The effect on I_2 dissociation is larger for $\Gamma/DV_\bullet = 8.0$ (about 33 percent at $x = 1.8$ cm). Even so, this is a relatively small variation considering the magnitude of the variation in the vortex strength.

Of all the experimental jet data, the jet trajectory information is the most accurate. If the predicted jet penetration is close to the nozzle centerline ($\eta = 0$), the symmetry condition at that location would probably influence the jet trajectory. However, for the conditions used here (Equation 4.1) the jet closest to the centerline (JET1) is still well away from it. Therefore, it is believed that the values used for the initial jet locations (Equation 2.30) are probably accurate. However, to see what impact the symmetry boundary condition at $\eta = 0$ would have, a case was run where the jet centerlines were moved towards $\eta = 0$ such that the large jet (JET1) was just touching the $\eta = 0$ boundary ($\eta_1 = 0.0814$ and $\eta_2 = 0.44153$). The results indicated negligible influence on the I_2 dissociation but the gain was strongly affected with the average gain being reduced from 0.0043/cm to 0.0026/cm at $x = 1.8$ cm. It is apparent, therefore, that for extreme variations in jet location, the calculated results will be strongly influenced.

It is believed that the results of this section demonstrate that the computed results are only moderately influenced by relatively large variations in the initial vorticity field. Large variations in jet location can influence the results, but there is little uncertainty in the jet location.

44
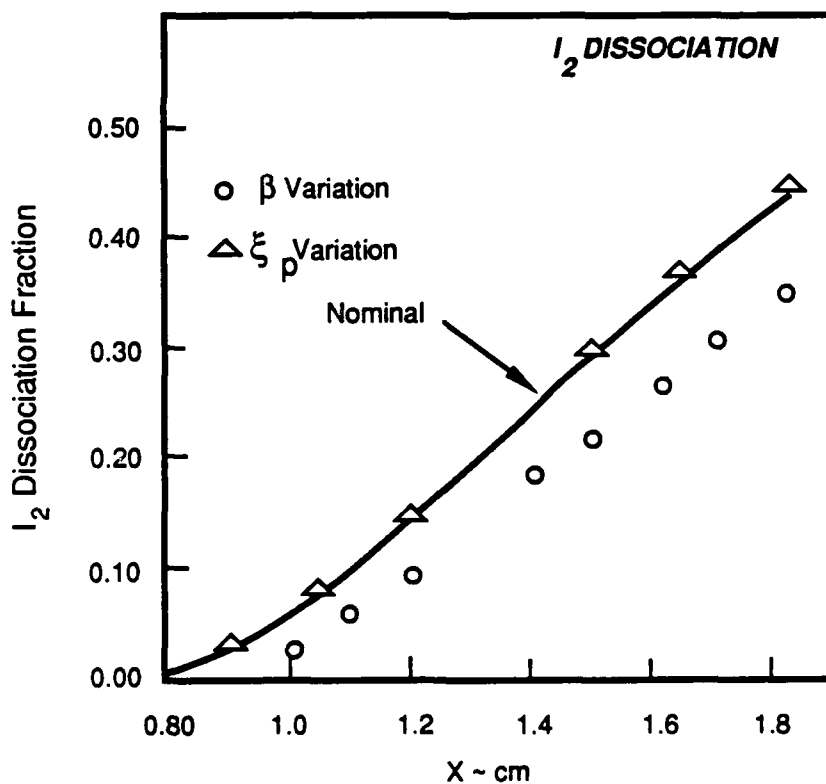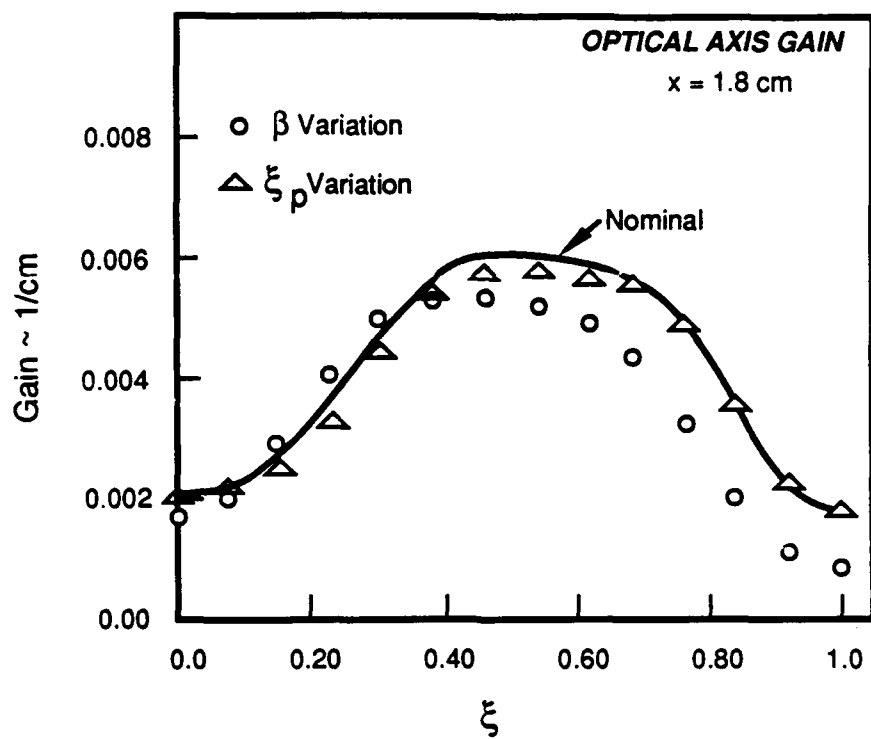
Figure 4.11. Influence of initial conditions on gain and iodine dissociation.

4.4 ZERO VORTICITY RESULTS.

Figure 4.12 showed that reducing the nominal vorticity by a factor of 2 had only a small influence on the computed results. The obvious question is, What would be the impact of zeroing the vorticity? If the results are only slightly affected when the initial vorticity is zeroed, it would suggest that the transverse velocity components could be ignored and the problem treated as a 3-D diffusion problem with a single convective velocity component (the axial velocity). The comparison with the initial vorticity zeroed is contained in Figure 4.13, which shows that the gain is strongly affected by zeroing the vorticity. It is concluded that the flow problem cannot be simplified by using a zero vorticity approximation.

Figure 4.12.   Influence of initial vortex strength on iodine
               dissociation and gain.

Figure 4.13.   Influence of zero vorticity on iodine dissociation
and gain.

SECTION 5

SUMMARY AND CONCLUSIONS

A 3-D fluid dynamic computer code (TRIMIX) has been written to analyze the mixing between a primary flow and a secondary flow injected as a series of discrete jets from the walls which bound the flow. The flow problem has been parabolized by starting the calculation just downstream of the jet injection location where the jets have been turned parallel to the primary flow. T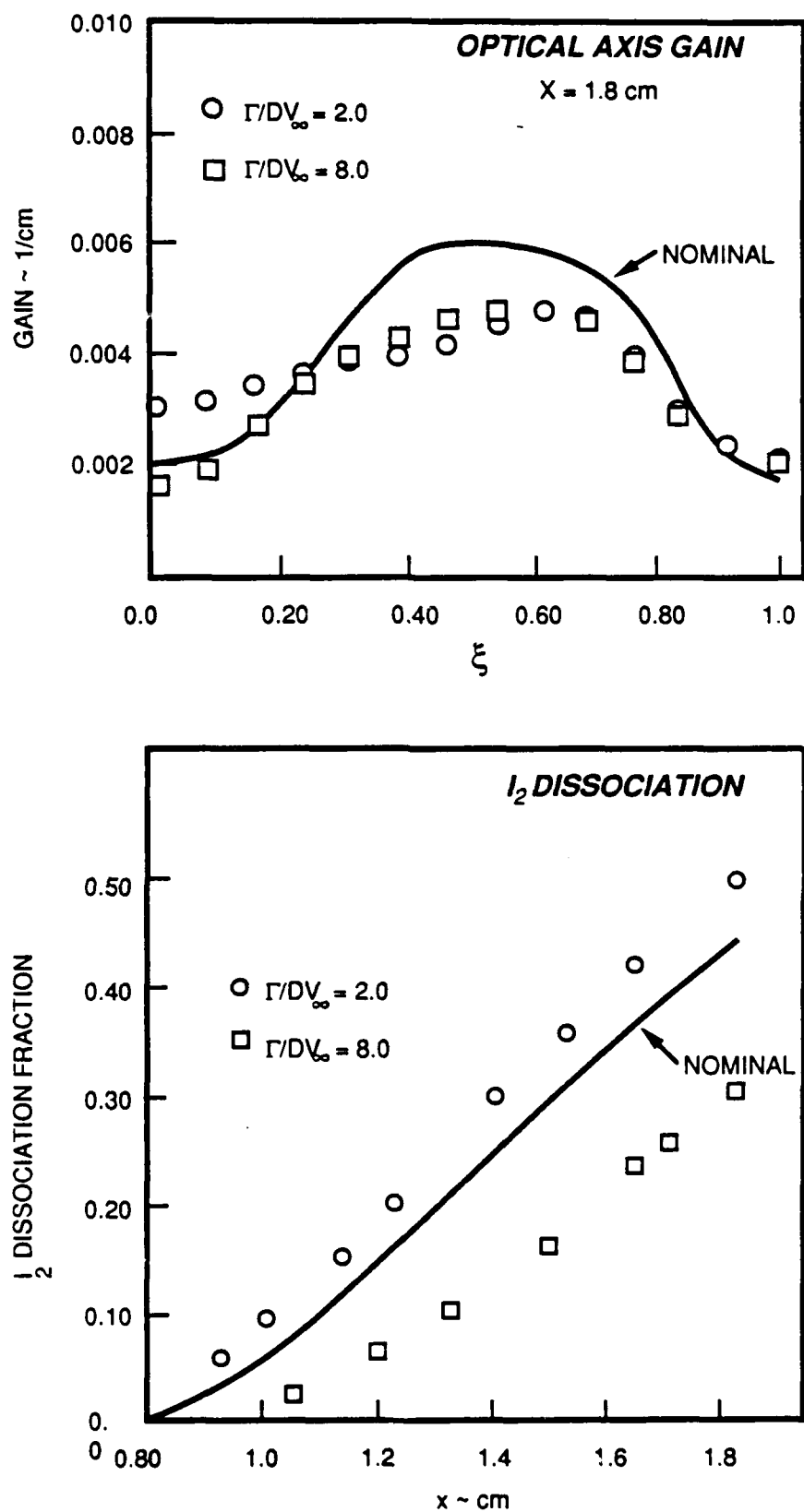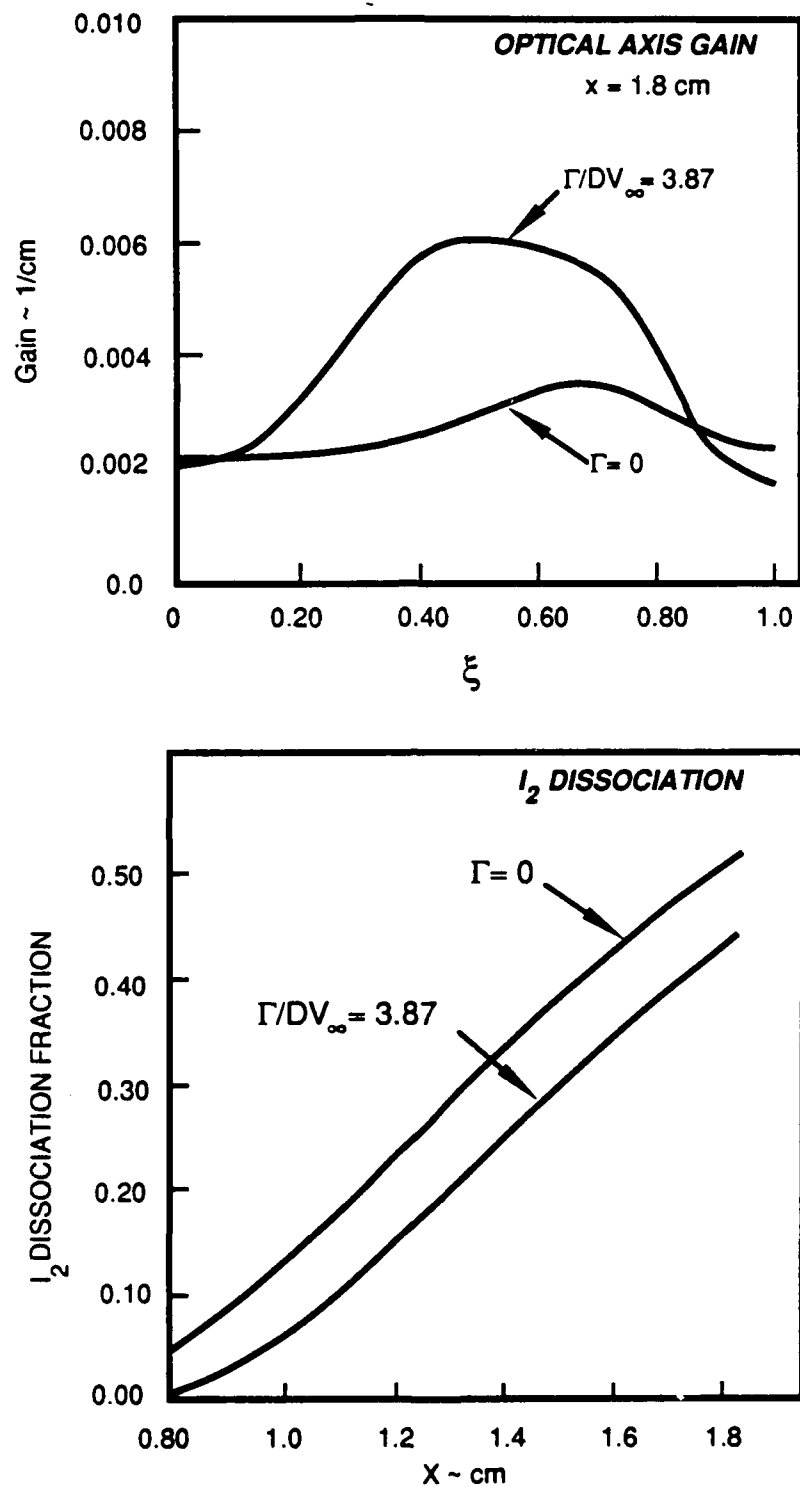he initial conditions at this location have been defined by assuming that the primary and secondary flows are pressure matched and unmixed. The equations are solved using a vorticity-stream function formulation and the initial distribution of axial vorticity is obtained from the experimental data base on jet injection.

A number of calculations have been carried out in a constant area flow channel which has been chosen to represent the subsonic portion of a RotoCOIL laser nozzle. The oxygen/iodine set of species and reactions consisting of 10 species and 21 reactions has been used for the calculation. The equations were solved over a rectangular grid containing 768 mesh points, and the required computation time on the CRAY 1 computer was about 2 h/cm of distance in the flow direction.

The calculations indicate that moderate uncertainties in the initial conditions have only a minor influence on the computed results. This finding provides the justification for the approach used in the TRIMIX code; namely, that the initial conditions can be specified accurately enough for meaningful results to be obtained from the calculation.

It has been demonstrated that the choice of diffusion model can have a significant influence on the results even for flows with large axial vorticity. This is in agreement with an identical comparison for 2-D mixing calculations with zero vorticity. It is

49

concluded that the use of the binary diffusion model should be abandoned in chemical laser mixing calculations.

Comparisons with the premixed model indicate that the use of the premixed assumption will significantly underpredict the amount of iodine dissociation and small signal gain. This result should put to rest the misconception that the premixed assumption always predicts the most optimistic laser performance. However, it has been shown that the use of the premixed model with the use of an artificially increased I_2 dissociation rate constant will give the correct average values for yield and gain. This result provides some justification for the use of the premixed model in situations where the degree of I_2 dissociation is known from experiments.

It is believed that the TRIMIX code provides a rational model for analyzing the performance of oxygen/iodine lasers at a reasonable computational cost. It includes the 3-D aspects (geometry and axial vorticity) which are ignored in 2-D codes and it is at least one and possibly two orders of magnitude faster than an exact Navier-Stokes code. However, the code does contain approximations in the definition of the starting conditions and it should be compared with both experimental data and a Navier-Stokes solution. Future effort should concentrate on adding the capability to solve the species equations simultaneously, addition of a resonator model for power extraction, and code validation efforts.

REFERENCES

1. Crowell, P., "Laminar Mixing Between Chemically Reacting Parallel Streams of Excited Oxygen and Iodine for an Exact Multicomponent Diffusion Model," RDA Report No. 83-A/K-14-0.1984, Albuquerque, NM, 21 April 1983.

2. Crowell, P., "A Comparison of the Effective Binary Diffusion and Multicomponent Diffusion Models for Laminar Mixing of Oxygen/Iodine Streams," RDA Report No. 83-A/K-14-0.2009, Albuquerque, NM, 16 May 1983.

3. Crowell, P., "The Effective Binary Diffusion Model," RDA Report No. 87-A/K-3-02-165, Albuquerque, NM, 27 October 1987.

4. Fearn, R. and R.P. Weston, _Vorticity Associated with a Jet in a Cross Flow_, J. AIAA, Vol. 12, No. 12, p. 1666, December 1974.

5. Karagozian, A. R., _An Analytical Model for the Vorticity Associated with a Transverse Jet_, J. AIAA, Vol 24, No. 3, p. 428, March 1986.

6. Truman, C. R., et al, "Noniterative Solutions for Pressure in Parabolic Flows," _Advances and Applications in CFD_, Vol. 66, pp 121-127, ASME/FED, December 1988.

7. Plummer, D., R. Heidner, and G. Perram, "The Proceedings from the Air Force Weapons Laboratory Conference on Chemical Oxygen-Iodine Laser Kinetics," Kirtland AFB, NM, March 1988.

8. Crowell, P., "RECOIL: A One-Dimensional Chemical Oxygen Iodine Laser Performance Model, Part I - Theory," RDA Report No. 87-A/K-3-02-1079, Albuquerque, NM, November 1989.

APPENDIX A

VORTICITY TRANSPORT EQUATION FOR A COMPRESSIBLE, VARIABLE VISCOSITY FLUID

The vorticity transport equation for an incompressible, constant viscosity fluid has a particularly simple form and may be found in many books. The corresponding result for nonconstant viscosity and a compressible fluid is difficult to locate and is presented in this appendix.

The vorticity and velocity are defined by:

$$\omega \equiv \nabla \times V = \omega_x e_x + \omega_y e_y + \omega_z e_z \tag{A.1}$$

$$V \equiv u e_x + v e_y + w e_z$$

The momentum equation for steady flow may be written as:

$$\rho \nabla \left(\frac{1}{2} V^2\right) - \rho V \times \omega = - \nabla p + \nabla(\mu \nabla V) \tag{A.2}$$

By taking the curl of Equation A.2 and combining with the continuity equation, the vorticity transport equation is obtained as:

$$(\rho V \cdot \nabla)\omega - (\omega \cdot \nabla)\rho V + \nabla\rho \times \nabla\left(\frac{1}{2} V^2\right)$$

$$\tag{A.3}$$

$$= \nabla(\mu \nabla \omega) - (\nabla\mu \cdot \nabla)\omega + \nabla \times [(\nabla\mu \cdot \nabla)V] + \nabla\mu \times \nabla^2 V$$

Equation A.3 is a vector relationship which provides the transport equations for the scalar components ω_x, ω_y and ω_z. Note that for constant density and viscosity, the gradients of ρ and μ vanish and the usual equation is recovered.

52

Since only the axial vorticity (ω_x) is solved for in the TRIMIX code, we express Equation A.3 for the scalar component ω_x as follows:

For notational convenience, we define:

$$\alpha \equiv \text{x component of:} \quad \nabla\rho \times \nabla\left(v^2/2\right) \tag{A.4}$$

$$\beta \equiv \text{x component of:} \quad \nabla\mu \times \nabla^2\mathbf{V} + \nabla\times[(\nabla\mu\cdot\nabla)\mathbf{V}] - (\nabla\mu\cdot\nabla)\omega$$

The scalar equation for ω_x is obtained as:

$$\rho\mathbf{V}\cdot\nabla\omega_x + \alpha = \nabla\cdot\left(\mu\nabla\omega_x\right) + \omega\cdot\nabla\rho u + \beta \tag{A.5}$$

Equation A.5 is parabolized by dropping the x derivatives in the expression for β and the x derivative in the divergence of $\mu\nabla\omega_x$.

The form of Equation A.5 which is solved for ω_x is given by:

$$\rho\mathbf{V}\cdot\nabla\omega_x = \nabla\cdot\left(\mu\nabla\omega_x\right) + \omega_x\frac{\partial}{\partial x}(\rho u) + \Omega \tag{A.6}$$

$$\Omega \equiv \omega_y\frac{\partial}{\partial y}(\rho u) + \omega_z\frac{\partial}{\partial z}(\rho u) + \beta - \alpha$$

The vorticity components in the y and z direction in the expression for Ω are calculated from the definitions of Equation (A.1). That is:

$$\omega_y = \frac{\partial u}{\partial z} - \frac{\partial w}{\partial x} \qquad\qquad \omega_z = \frac{\partial v}{\partial x} - \frac{\partial u}{\partial y} \tag{A.7}$$

APPENDIX B
INITIAL CONDITIONS

In this appendix, the global conservation equations for mass, momentum and energy are used in conjunction with some closure assumptions to determine the initial flow conditions at station D (see Figure 2.2).

The axial momentum equation at station D may be written as:

$$\left(P_m A\right)_D = \left(P_m A\right)_p + \left(P_m A\right)_1 + \left(P_m A\right)_2 \qquad (B.1)$$

$$P_m \equiv P + \rho u^2$$

where subscript p refers to the primary flow and subscript 1 and 2 refer to the injected jets.

The flow area at station D must be conserved such that:

$$A = A_p + A_1 + A_2 \qquad (B.2)$$

Assuming normal injection, such that the jets add nothing to the axial momentum, and ignoring wall friction, the momentum at station O and D is equal. That is,

$$\left(P_m A\right)_D = \left(P_m A\right)_O \qquad (B.3)$$

Ignoring heat transfer between the primary flow and the injected jets, the total temperatures at station D are known. The energy equation for the jets and the primary are given by:

$$T_{op} = T_p \left(1 + (\gamma_p - 1) M_p^2 / 2\right)$$

$$T_{os} = T_1 \left(1 + (\gamma_s - 1) M_1^2 / 2 \right) \qquad (B.4)$$

$$T_{os} = T_2 \left(1 + (\gamma_s - 1) M_2^2 / 2 \right)$$

where T_{op} is the primary flow total temperature at station O, and T_{os} is the plenum temperature for the jets. Subscript s refers to the secondary flow (i.e., the jets).

Since there is assumed to be no mixing between the injection locations and station D, the mass flows are given by:

$$\dot{m}_p = (\rho UA)_p$$

$$\dot{m}_1 = (\rho UA)_1 \qquad (B.5)$$

$$\dot{m}_2 = (\rho UA)_2$$

Since both jets are fed from a common plenum, the jet mass flows are related by the ratio of the injection hole areas. That is,

$$\dot{m}_1 = \dot{m}_2 \left(A_1 / A_2 \right)_{inj} \qquad (B.6)$$

With the assumption that the flows are pressure equilibrated at station D, the pressures are given by:

$$P_p = P_1 = P_2 = P \qquad (B.7)$$

To close the system of equations, a value for the ratio of the jet areas at station D must be assumed. The obvious choice is to use the same ratio as the hole pattern. This gives:

$$A_1 / A_2 = \left(A_1 / A_2 \right)_{inj} \qquad (B.8)$$

The given information consists of $(P_m A)_o$, T_{op}, T_{os}, $\dot{m}_p$, $\dot{m}_1$, $\dot{m}_2$, $(A_1/A_2)_{inj}$ and the area A at station D. For given values of A_1/A_2 and the pressure P, all the flow values and the areas occupied by the jets and primary may be calculated at station D. As indicated, Equation (B.8) is used for the jet area ratio. The pressure P is obtained by assuming that it is the same value as the premixed pressure. The premixed pressure is easily calculated by assuming instantaneous mixing of the jets and primary without chemical reactions. The premixed conservation equations for mass, momentum and energy are easily derived and are not repeated here.

To solve the system of equations, an iterative solution is required where the Mach number M_1 is the iteration parameter. Note that the choice for the jet area ratio (Eq. B.8) dictates that $M_2 = M_1$ and therefore the properties (temperature, velocity and density) of both jets are identical.

To summarize: With the assumption of negligible mixing and heat transfer and rapid pressure equilibration between the jets and the primary, the global conservation equations may be solved to obtain the initial condition for the 3-D parabolic mixing calculation. It is believed that these approximations and the closure assumptions of premixed pressure and Equation (B.8) for the jet area ratio are reasonable. To assess the accuracy of these approximations would require generating some exact 3-D solutions of the Navier-Stokes equations for comparison purposes.

APPENDIX C

GAIN MODEL

The gain is dependent upon the density, temperature and I and I*
concentrations and is obtained from Equation C.20 and C.17 of
Reference C.1.

$$\alpha = \lambda^2 A_{21} G \ [N_2 - g_2 N_1 / g_1] / 8\pi \qquad (C.1)$$

where λ is the wavelength and A_{21} is the Einstein coefficient for
spontaneous emission. The line shape function, G, is obtained from
the Voight function and includes both the effects of Doppler and
pressure broadening. Pressure broadening was included in the gain
calculation through the use of experimental pressure broadening
coefficients obtained from the literature.

Schlie (Ref. C.2) reports that the laser should operate on the 3-4
hyperfine transition and this is assumed to be the case here. For
this transition, the number densities of the upper and lower states
are related to the total number density of I and I* by the
following (Ref. C.2):

$$N_1 = 9N_I / 24$$

$$\qquad (C.2)$$

$$N_2 = 7N_{I*} / 12$$

where the number density of any species is related to its mass
fraction by:

$$N_i = N_A \ \rho K_i / M_i \qquad (C.3)$$

where N_A is Avogadro's number and M_i is the molecular weight of
species i.

The degeneracy ratio and the Einstein coefficient are (Ref. C.2):

$$g_2 = 7g_1 / 9 \qquad\qquad A_{21} = 5.0 \ s^{-1} \qquad (C.4)$$

The Voight (Ref. C.3) line shape function is given by:

$$G = \frac{2}{\Delta v_D} \quad \frac{\ln 2}{\pi} \ [1 - \text{erf}(y)] \ \text{EXP}(y^2)$$

(C.5)

$$y = \Delta v_L \ \sqrt{\ln 2}/\Delta v_D$$

where Δv_L and Δv_D are the Lorentz and Doppler full-width, half maximum line shape. The Doppler width is given by:

$$\Delta v_D = 2(2RT\ln 2/M)^{1/2}/\lambda$$

(C.6)

For pressure broadening, the line width (Eq. 4.8 of Ref. C.1) is proportional to the collision frequency (the inverse of the average time between collisions). Using the expression of Reference C.4 (page 1023) for the collision frequency, the Lorentz line width may be expressed as:

$$\Delta v_L = \left(\frac{T_r}{T}\right)^{1/2} \sum \beta_{ai} P_i$$

(C.7)

$$\beta_{ai} = \frac{2N_A Q_{ai}}{\pi^2} \frac{2\pi}{RT_r} \left(\frac{1}{M_a} + \frac{1}{M_i}\right)^{1/2}$$

where T_r is any reference temperature, N_A is Avogadro's number, and M_a and M_i are the molecular weights of species a and i. Q_{ai} is the optical cross section, and P_i is the partial pressure of species i.

Generally, an expression for the optical cross section Q_{ai} is not available, and the Lorentz width is evaluated from measured pressure-broadening coefficients. The literature values (denoted by α_{ai}) are usually presented in a manner which implies no temperature dependence on Δv_L. That is,

$$\Delta v_L = \sum \alpha_{ai} P_i$$

(C.8)

The β_{ai} coefficients are related to the measured literature values of α_{ai} by:

$$\beta_{ai} = \alpha_{ai} \left(\frac{T_m}{T_r}\right)^n \qquad \text{(C.9)}$$

where T_m is the measured gas temperature at which α_{ai} was determined.

If the optical cross section is independent of temperature, then n = 0.50 from Equation C.7. On page 1025 of Reference C.4 it is stated that Q_{ai} is inversely proportional to the square root of temperature. If so, then it follows that n = 1.0. If the measured α_{ai} are available at room temperature, then by choosing the reference temperature equal to room temperature (i.e., T_r = 295 K) we have $\beta_{ai} = \alpha_{ai}$. This is the approach used in the code: the β_{ai} are taken to be the measured room temperature values and Equation C.7 is used to calculate the Lorentz width.

REFERENCES

C.1. Lengyel, B., <u>Lasers, 2nd Edition,</u> John Wiley and Sons, 1971.

C.2. Schlie, L.A., "Anomalous Dispersion Effects in Atomic Iodine Chemical Laser at 1.315 μm," <u>Laser Digest</u>, pp. 112-162, AFWL-TR-80-146, Kirtland AFB, NM, March 1981.

C.3. Gross, R. and J. Bott, <u>Handbook of Chemical Lasers</u>, pp. 488-490, John Wiley and Sons, 1976.

C.4. Hirschfelder, J., C. Curtiss and R. Bird, <u>Molecular Theory of Gases and Liquids</u>, John Wiley and Sons, 1954.